A Semi-Analytic Approach to Baroclinic Instability on the African Easterly Jet

Jesse Norris

August 2010

Abstract

In this study an idealised semi-analytic model is used to simulate baroclinic insta-bility on the African easterly jet (AEJ) and model the time evolution of potential vortcity (PV) waves on the basic state. Work in the literature has focussed on mid-latitude westerly jets so the analysis of an idealised easterly jet is new. Using analytically calculated Green functions, the PV structure is inverted at each time step to obtain the meridional winds. The meridional flow advects the basic state PV, thus affecting the evolution of PV waves. The time integration is performed numerically. It is shown that the curvature of the AEJ is sufficient to cancel the planetary meridional vorticity gradient β and hence create a negative meridional PV gradient somewhere below the jet core. Therefore a pair of counter-propagating Rossby waves (CRW's) can exist and mutual growth can occur. One CRW is a westward propagating wave formed on the positive meridional temperature gradient at the ground, the other an eastward propagating wave formed on the negative PV gradient in the interior. The wavelength with the fastest growing normal mode is found to be approximately 1500km. With an initial perturbation given 5 days to develop, the total energy growth is found to be highly sensitive to the initial PV structure with the optimal perturbation over this time strongly resembling a tilted monopole. Phase-locking of CRW's within the allowed time is shown to be possible but the energy growth is strongly dominated by linear transient mechanisms during this time.

Acknowledgements

This study would not have been possible without the great help of my supervisor John Methven who has remained contactable and highly approachable throughout. He has always given however much time necessary to help me to understand the various complex concepts that I initially struggled to understand. Feedback on my progress has also been extremely helpful. Thanks are given to Hylke de Vries who has written the highly detailed code for the model that has been used here and inserted very helpful comments to explain how the various components work, thus allowing me to write the relevant modifications. I have also had help from Emma Irvine to get to grips with the model who has been thoroughly approachable. Finally, thanks go to the NERC for funding my place on the Mathematical and Numerical Modelling of the Atmosphere and Oceans Msc this year.

Declaration

I confirm that this is my own work and the use of all materials from other sources have been properly and fully acknowledged.

Signed .... 　　　 Date ....

Contents

1 Introduction

1.1 The African Easterly Jet

A jet stream is a fast zonal air current caused by a large meridional gradient of potential temperature (PT) $\left| \frac{\partial \theta}{\partial y} \right| >> 0$ in thermal wind balance:

$$f \frac{\partial \bar{u}}{\partial z} = -\frac{g}{\theta_0} \frac{\partial \theta}{\partial y} \tag{1}$$

with an increase or decrease of zonal velocity with height $\frac{\partial \bar{u}}{\partial z}$, where zonal velocity $\bar{u}$ is positive if it is eastward. In (1), $f = 2\Omega \sin\phi$ is the Coriolis parameter, $g = 9.81 \text{ms}^{-2}$ is acceleration due to gravity, θ_0 is a reference value for PT, $\Omega = 7.292 \times 10^{-5} \text{s}^{-1}$ is the rate of the Earth's rotation and ϕ is latitude. The PT is given by:

$$\theta = T \left(\frac{p}{p_0} \right)^{R/c_p} \tag{2}$$

where T is absolute temperature, p is pressure, p_0 is a reference value for pressure, R is a gas constant for air and c_p is specific heat capacity at constant pressure. For adiabatic flow, PT is conserved following air parcels and and the pressure factor accounts for decreasing temperature in adiabatic expansion.

In the Northern Hemisphere, $f > 0$, implying that a positive potential temperature gradient $\frac{\partial \theta}{\partial y} > 0$ is associated with a negative zonal wind shear $\frac{\partial \bar{u}}{\partial z} < 0$ and vice versa.

It is normally the case in the Northern Hemisphere that $\frac{\partial \theta}{\partial y} < 0$ (temperature decreases from equator to pole), which, if the gradient is sufficient, implies a significant increase in velocity with height. This is known as a westerly jet stream (eastward winds).

In North Africa, however, the Sahara desert is much warmer than the region immediately south of it. Therefore, due to the large positive PT gradient, (1) implies a negative zonal wind shear, i.e. wind speed becoming more easterly (westward) with height. This is the **African Easterly Jet** (AEJ), a lower tropospheric westward air current flowing along the southern edge of the Sahara at approximately 16°N latitude from Ethiopia (40°E) to the west African coast (15°W) . It has a jet core at approximately 650 hPa (4km altitude) where mean wind speed is 12ms^{-1} (Thorncroft *et al.* (2008)). **African Easterly Waves** (AEW's) are meridional undulations
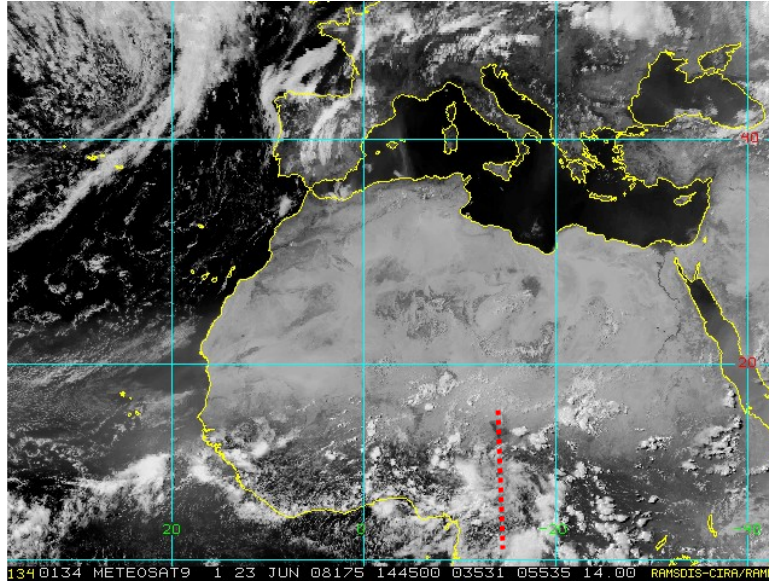
Figure 1:

Thermal satellite image showing cloud tops along the African easterly jet. Image taken from
http://www.wunderground.com/blog/Drakoen/archive.html?year=2008month=06.

in the AEJ, bringing moist air from the equatorial coastline to the south and dry air from the Sahara desert to the north. This results in the distinctive cloud pattern shown in Figure 1. The convection in the moist air brings most of the rainfall to the arid Sahara region. As the winds in the jet are responsible for transporting moisture across west Africa, such perturbations can determine where and when there is rainfall in the region. AEW's are observed to propagate west along the AEJ and a small number of storms embedded within them develop into tropical cyclones as they leave the continent, gaining energy from the Atlantic ocean and form some of the hurricanes reaching North America. Therefore the mechanisms behind AEW's are of great interest from a research perspective in order to describe their evolution and hence forecast both the region's weather and the development of tropical cyclones.

Waves are common to all jet streams and are known as atmospheric **Rossby waves** which are created by potential vorticity (PV) anomalies as will be described in Section 2. Following Bretherton (1966), a single Rossby wave is neutral (does not grow) by itself but growth can occur, depending on the stability of the atmosphere, via the interaction of two Rossby waves propagating in opposite directions.

2

It will be shown that, if certain conditions are satisfied, these two waves eventually phase-lock and mutually grow exponentially. Such pairs of waves are known as **counter-propagating Rossby waves** (CRW's) and form the basis of this study.

1.2 Aims of this study

Almost all the research on growth via CRW interaction has been for westerly jets and as we shall see there is a profound asymmetry between easterly and westerly jets due to the meridional Coriolis gradient $\beta = \frac{df}{dy}$ which makes easterly jets more stable. Easterly jets will be the focus of this study. As will be shown in Section 2, due to the positive temperature gradient at the ground below the AEJ, a pair of mutually growing CRW's is not possible unless curvature of the jet profile is sufficient to overwhelm the positive β. Sustained exponential growth can only occur if the pair of CRW's phase-lock in a mutually amplifying configuration - the growing normal mode. Therefore the first thing that must be established for any study on CRW interaction on the AEJ is that the jet curvature is indeed strong enough. For the purposes of this particular study, we are specifically interested in the following questions:

1. For which wavelengths do normal modes grow most rapidly on an easterly jet and how quickly do they propagate? Also, how does this behaviour contrast with a westerly jet with the same structure but opposite sign?

2. How sensitive is the evolution of the system to the initial perturbation and what is the nature of the optimal perturbation for which energy growth is greatest?

3. Given the finite-time available for Rossby waves to propagate along the AEJ, t_{AEJ}, do CRW's have sufficient time to phase-lock and, if so, how much of the total energy growth is attributable to transient changes in PV structure as opposed to modal growth?

1.3 Relevant scaling

Before describing the mathematics of CRW's, it is necessary to establish some of the constants and scales that will be used throughout this study: At 16°N, the latitude of the AEJ, we have the following:

$$f = 2\Omega\sin(16°) = 4.02 \times 10^{-5}\text{s}^{-1} \tag{3}$$

$$\beta = \frac{df}{dy} = \frac{df}{d\phi}\frac{d\phi}{dy} = \frac{2\Omega\cos(16°)}{a} = 2.20 \times 10^{-11}\text{m}^{-1}\text{s}^{-1} \tag{4}$$

where $a = 6.37 \times 10^6$m is the mean radius of the Earth. Following the literature, the Brunt-Vaisala frequency:

$$N = \sqrt{\frac{g}{\theta_0}\frac{\partial\theta}{\partial z}} \approx 0.01\text{s}^{-1} \tag{5}$$

is taken to be constant at the above value to good approximation throughout the atmosphere. We introduce a magnitude for the vertical wind shear:

$$\Lambda = 3 \times 10^{-3}\text{s}^{-1} \tag{6}$$

so that $\frac{d\bar{u}}{dz} = \Lambda\frac{d\hat{u}}{d\hat{z}}$, where $\hat{z},\hat{u}$ are the non-dimensional height and zonal velocity respectively. Height z is non-dimensionalised, following Held (1978), as follows:

$$H_z = \frac{f^2\Lambda}{N^2\beta} = 2.2\text{km} \tag{7}$$

so that $z = H_z\hat{z}$ and we will see in due course that, algebraically, this is a very useful scale to use. The corresponding velocity scale is thus:

$$U = \Lambda H_z = 6.6\text{ms}^{-1} \tag{8}$$

where $\bar{u} = U\hat{u}$. Assuming Burger number $\frac{NH}{fL} = 1$, we use the natural length-scale:

$$L = \frac{N}{f_0}H_z = 547\text{km} \tag{9}$$

where $x = L\hat{x}$ and $\hat{x}$ is the non-dimensional zonal co-ordinate. And hence the advective time scale is:

$$T = \frac{L}{U} = 82,919\text{s} \approx 1 \text{ day} \tag{10}$$

where $t = T\hat{t}$. The length of the AEJ is approximately:

$$L_{\text{AEJ}} \approx 5000 \text{ km} \tag{11}$$

and hence the non-dimensional minimum time available for waves to propagate along the jet is given by:

$$t_{\text{AEJ}} = \frac{L_{\text{AEJ}}}{u_{\text{AEJ}}T} = 5.03 \tag{12}$$

where $u_{\text{AEJ}} = 12\text{ms}^{-1}$ is the mean speed at the jet core. We also non-dimensionalise wavenumber and wavelength as follows. The angular wavenumber is given by:

$$k = \frac{2\pi L}{\lambda} \tag{13}$$

We non-dimensionalise wavelength by:

$$\lambda = 4\pi Lr \tag{14}$$

where wavelength:

$$r = \frac{1}{2k} \tag{15}$$

is the parameter used in the Charney model (Charney (1947)) as will be studied in Section 2. Finally, we introduce a density height scale H_ρ such that the non-dimensional density is given by:

$$\rho = \rho_0 e^{-z/H_\rho} \tag{16}$$

In order to establish the value of H_ρ, we note the equation for hydrostatic balance:

$$dp = -\rho g dz \tag{17}$$

where p is pressure. Using the ideal gas equation:

$$p = \rho RT \tag{18}$$

where $R = 287\text{JK}^{-1}\text{kmol}^{-1}$ is the gas constant for the atmosphere, (17) becomes:

$$\frac{dp}{p} \approx -\frac{gdz}{RT_0} \tag{19}$$

where T_0 is a reference temperature, provided that temperature variations are small compared to temperature values $\delta T << T$. Hence:

$$H_\rho \approx \frac{RT_0}{g} = 7.7\text{km} \tag{20}$$

for average temperature in profile above west Africa $T_0 \approx 260\text{K}$.

1.4 Quasi-geostrophic theory

For geostrophic balance, where the horizontal pressure gradient and Coriolis forces are balanced, the zonal and meridional wind components u and v are as follows (Pedlosky(1990)):

$$u = -\frac{\partial \psi}{\partial y} \quad v = \frac{\partial \psi}{\partial x} \tag{21}$$

where the geostrophic streamfunction is given by:

$$\psi = \frac{p'}{\rho f_0} \tag{22}$$

for a pressure perturbation p'. The vertical component of geostrophic relative vorticity is then given by:

$$\xi = \frac{\partial v}{\partial x} - \frac{\partial u}{\partial y} = \frac{\partial^2 \psi}{\partial x^2} + \frac{\partial^2 \psi}{\partial y^2} \tag{23}$$

For hydrostatic balance, where the vertical pressure gradient is balanced by gravity, the buoyancy is given by:

$$b' = f_0 \frac{\partial \psi}{\partial z} \tag{24}$$

where the buoyancy is defined as:

$$b' = \frac{g\theta'}{\theta_0} \tag{25}$$

From (2) and (25), we see that T, θ and b' are all positively correlated so that hereafter we shall refer to anomalies of temperature, PT and buoyancy interchangably. From (21) and (24), thermal wind balance follows, where in this case we are just interested in thermal wind balance for a meridional temeprature gradient (1).

Quasi-geostrophic (QG) theory applies to an atmosphere that can be taken to be in geostrophic balance to good approximation but where the evolution of the geostrophic variables ξ and b' is related to the ageostrophic wind components $u_{\mathrm{ag}}, v_{\mathrm{ag}}, w$ where $u + u_{\mathrm{ag}}$ gives the full zonal velocity (and similarly for v) and w is the vertical velocity. We define $\zeta = f + \xi$ as the vertical component of absolute (planetary plus relative) vorticity with the notion that stretching (contracting) the vortex results in an increase (decrease) of absolute vorticity:

$$D\zeta = \frac{f_0}{\rho} \frac{\partial}{\partial z} (\rho w) \tag{26}$$

where D denotes the total derivative $\frac{\partial}{\partial t} + u\frac{\partial}{\partial x} + v\frac{\partial}{\partial y}$, i.e. the rate of change following the (in this case geostrophic) flow. It is also the case that advection of PT surfaces through the vertical results in buoyancy anomalies, expressed by the thermodynamic equation:

$$Db' = -N^2 w \tag{27}$$

From (26) and (27), we obtain the QG **potential vorticity** (PV) equation:

$$Dq = 0 \tag{28}$$

where QG PV (hereafter referred to as PV) is given by:

$$q = f + \xi + \frac{f_0}{\rho}\frac{\partial}{\partial z}\left(\frac{\rho b'}{N^2}\right) \tag{29}$$

1.5 Potential vorticity

Substituting (24) into (29), we obtain:

$$q = f_0 + \beta y + \frac{\partial^2 \psi}{\partial x^2} + \frac{\partial^2 \psi}{\partial y^2} + \frac{1}{\rho}\frac{\partial}{\partial z}\left(\frac{f_0^2 \rho}{N^2}\frac{\partial \psi}{\partial z}\right) \tag{30}$$

This means that PV is equal to the planetary vorticity $f_0 + \beta y$ plus the curvature of the local flow, assuming geostrophic and hydrostatic balance. We thus write $q = f + q'$ where $q' = \frac{\partial^2 \psi}{\partial x^2} + \frac{\partial^2 \psi}{\partial y^2} + \frac{1}{\rho}\frac{\partial}{\partial z}\left(\frac{f_0^2 \rho}{N^2}\frac{\partial \psi}{\partial z}\right)$ and hence, referring to the differential operator on ψ as ℓ:

$$\psi = \ell^-1(q - f) \tag{31}$$

i.e. the geostrophic streamfunction (hereafter streamfunction) is obtained by inverting the given differential operator. By considering (31) and (21), we see that a PV anomaly can influence the flow at distant points via the winds that it induces. This is a crucial concept for this study.

From (28), PV is conserved following the geostrophic flow in the absence of friction or diabatic effects. Thus it is a convenient variable to consider for initial value problems where we assume no friction or diabatic heating (as will be done throughout this study). If we define a basic state as the background flow at a particular location in the absence of a perturbation then (28) can be used to describe the evolution of some perturbation from the basic state. In stability studies the basic state is normally taken to be zonally symmetric and steady so that $\bar{u} = \bar{u}(y, z)$. The basic state

is also specified by the unperturbed PV $\bar{q}(y, z)$. Putting $q = \bar{q}(y, z) + q'(x, y, z, t)$ and linearising (28), we obtain:

$$\frac{\partial q}{\partial t} + \bar{u}\frac{\partial q}{\partial t} + v\bar{q}_y = 0 \tag{32}$$

where, in (32) and hereafter, q refers to the *perturbation* PV. (32) describes the evolution of PV q and its induced perturbation meridional wind v from a basic state defined by $\bar{u}$ and $\bar{q}_y$. We thus turn our attention to the nature of such PV perturbations.

2 Growing waves on jets

2.1 Counter-propagating Rossby waves

Consider a positive meridional PV gradient in the x-y plane ($\bar{q}_y > 0$), as depicted in Figure 2 where x and y are the zonal and meridional co-ordinates. If an air parcel is displaced to the south (i.e. into an area of lower PV than itself, due to the positive PV gradient), it creates a **positive PV anomaly** and forms a **Rossby wave**, i.e. a wave in the PV contours as shown. A positive PV anomaly induces increased cyclonic (anti-clockwise) rotation in its new environment. This implies that air is advected from the north (high PV) on the left flank of the anomaly and from the south (low PV) on the right flank of the anomaly. Thus the positive PV anomaly is shifted westwards.

Similarly, a **negative PV anomaly** (an air parcel displaced to the north into an area of higher PV than itself) induces increased anti-cylonic (clockwise) rotation in its new environment. This implies that that air is advected from the south (low PV) on the left flank of the anomaly and from the north (high PV) on the right flank of the anomaly. Thus the negative PV anomaly is also shifted to the left. Therefore
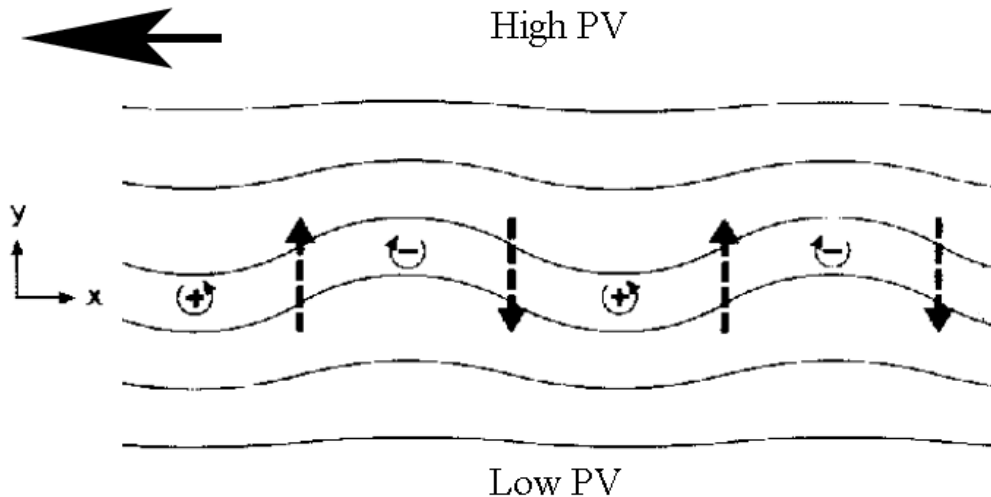

Figure 2: A Rossby wave forming on a positive PV gradient and hence propagating westward. Taken from Hoskins *et al.* (1985).

a Rossby wave formed on a *positive* PV gradient propagates *west* relative to the background zonal flow $\bar{u}$ as the above process is continued indefinitely. By a reverse

argument, a Rossby wave formed on a *negative* PV gradient ($\bar{q}_y < 0$) propagates *east* relative to $\bar{u}$.

Now consider the situation shown in Figure 3, where one Rossby wave is formed on a positive PV gradient and another is formed at a different latitude on a negative PV gradient. In this case, the wave formed where $\bar{q}_y < 0$ (wave 1) is propagating to the right relative to $\bar{u}$ and the wave where $\bar{q}_y > 0$ (wave 2) is propagating to the left relative to $\bar{u}$. They are hence known as **counter-propagating Rossby waves** (CRW's). If the two CRW's are at sufficiently close latitudes to interact then the meridional advection of air parcels associated with each wave (due to the PV anomalies as described above) is felt at the *home-base* of the other. In Figure
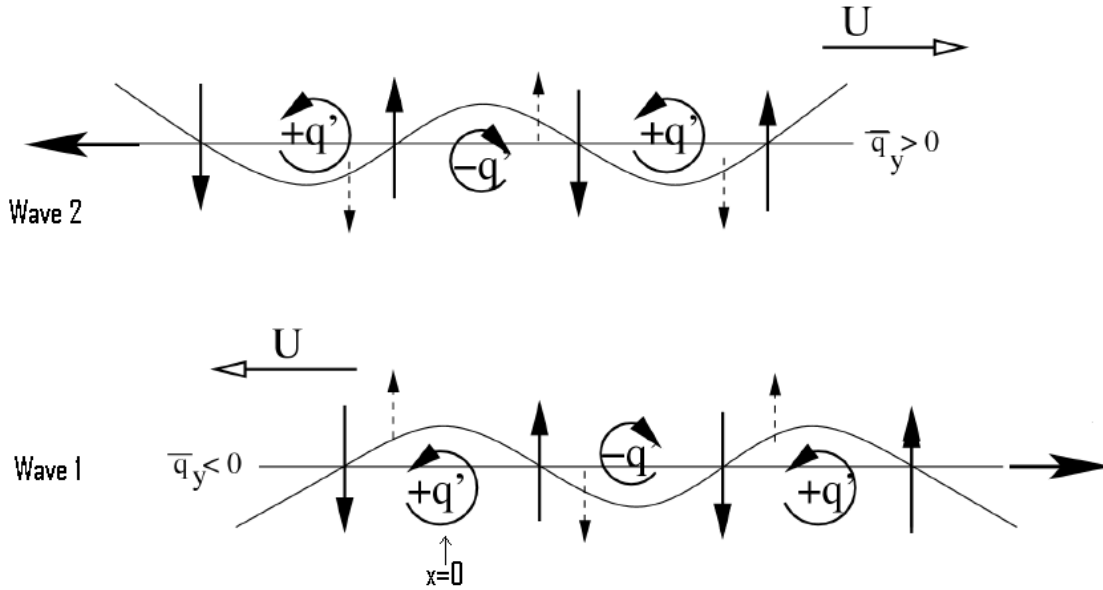
Figure 3: Counter-propagating Rossby waves with a phase difference between $\frac{\pi}{2}$ and π that leads to mutual growth and hindering of each's propagation direction. Bold horizontal arrows indicate each wave's propagation direction in the absence of interaction. Horizontal arrows labelled U indicate the advection of the wave due to the background zonal flow, relative to mid-channel flow. Bold vertical arrows indicate meridional air parcel advection due to the CRW at that location, dotted vertical arrows indicate air parcel advection due to the other CRW. Taken from Heifetz and Methven (2005).

3, the positive PV anomalies of wave 2 are between a quarter and a half wavelength to the left of the positive PV anomalies of wave 1. We say the phase difference

$\epsilon = \epsilon_2 - \epsilon_1$ (where $\epsilon_i = kx_i$ and the $x = 0$ at the positive anomaly of wave 1) is between $\frac{\pi}{2}$ and π. Following the arguments of Hoskins *et al.* (1985), in this particular configuration, negative PV air at home-base 2 is advected north (by the flow induced by wave 1) where there is already a negative PV anomaly at wave 2. Thus the negative anomaly of wave 2 is amplified. However, this occurs slightly right of the centre of the negative anomaly of wave 2, thus forcing the anomaly to the right and so hindering its tendency to propagate to the left.

Similarly, the advection of air parcels from wave 2 that is felt at wave 1 acts to amplify the negative anomaly there but reduce its propagation to the right. The net effect is that the two CRW's mutually amplify one another and *hinder* their counter-propagation.

Applying the same argument to the configuration where $0 < \epsilon < \frac{\pi}{2}$, we find that the two CRW's also mutually amplify one another but act to shift one another's negative anomalies in the direction they are already propagating, so that the CRW's propagate more rapidly in their opposite directions. Thus the interaction *helps* the counter-propagation.

Thus, for $0 < \epsilon < \pi$, a large ϵ causes the CRW's to hinder each other and so reduce ϵ, while a small ϵ causes the CRW's to help each other and so increase ϵ as summarised in 4. The CRW's therefore converge to some ϵ in this range where they phase-lock and so propagate with the same phase speed (including the effect of the interaction). As mutual amplification occurs for all phase differences in this region, the waves continue to grow indefinitely when in their phase-locked configuration. This is known as the **growing normal mode** (GNM).

Similarly, for an initial ϵ between 0 and $-\pi$, the CRW's mutually decay by each advecting high PV air to where the other has a negative anomaly. It also follows that the CRW's hinder each other for $-\pi < \epsilon < -\frac{\pi}{2}$ and help each other for $-\frac{\pi}{2} < \epsilon < 0$. Therefore the CRW's can phase-lock at some negative ϵ and continue to decay indefinitely. Thus is known as the **decaying normal mode** (DNM). However, this is an unstable fixed point in the phase diagram (Figure 4).

Thus we see that either the GNM or DNM is reached if the below condition, known as the Charney-Stern criterion for instability (Charney and Stern (1962)) , is satis-

fied:

$$q_y < 0 \text{ for CRW1} \quad \text{and} \quad q_y > 0 \text{ for CRW2} \tag{33}$$

where the numbering of the CRW's is arbitrary. In reality the background zonal flow $\bar{u}$ is different at the locations of the two waves. If $\bar{u}_{q_y<0} > \bar{u}_{q_y>0}$, i.e. the background flow is greater (more positive) where the PV gradient is negative than where it is positive, then each CRW initially propagates in the same direction as the relative zonal flow and so wave 1 is forced to the right of wave 2. This means ϵ is made negative whatever the initial phase difference and so the CRW's cannot phase-lock. If however:

$$\bar{u}_{q_y>0} > \bar{u}_{q_y<0} \tag{34}$$

as is pictured in Figure 3, then the wind shear forces wave 2 to the right of wave 1 ($\epsilon > 0$) and the GNM is eventually reached, whatever the initial phase difference. (34) is known as the Fjortoft criterion for instability (Fjørtoft (1950)). The situation
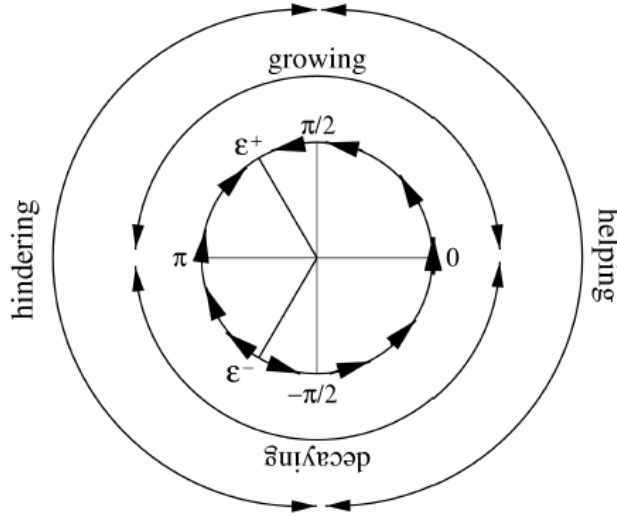
Figure 4: A summary of the mutual growth/decay and mutual helping/hindering for all CRW phase differences in the situation where (33) and (34) are satisfied, taken from Heifetz *et al.* (2004a). The arrows in the innermost circle indicate convergence to ϵ^+, the phase difference in the GNM(ϵ^- denotes the phase difference in the DNM). In this case $\frac{\pi}{2} < \epsilon^+ < \pi$ and $-\pi < \epsilon^- < -\frac{\pi}{2}$.

where two CRW's form at locations sufficiently close to interact and where (33) and (34) are satisfied is called **shear instability**. If two CRW's satisfying (33) and (34) are formed at different latitudes as described and so interact across the y-axis

then the shear instability described is called **barotropic instability**. Alternatively, two CRW's may be formed at the same latitude but at different altitudes and so interact in the vertical (across the z-axis). In this case the meridional advection of air parcels associated with each CRW is felt higher up (or lower down) at the other, as illustrated in Figure 5. In this case it is called **baroclinic instability**. In reality growth occurs via a combination of barotropic and baroclinic instability. However, for the purposes of this study we are solely concerned with baroclinic instability.
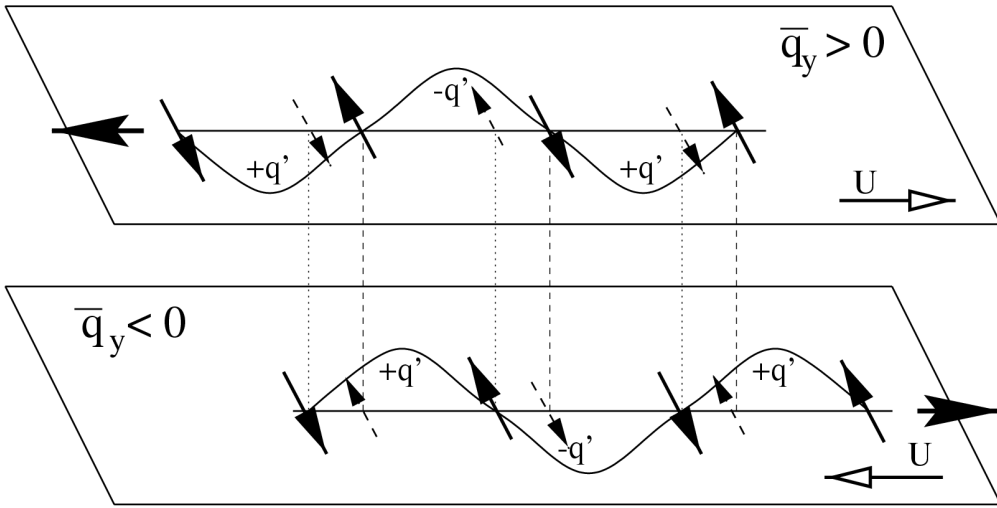

Figure 5: Counter-propagating Rossby waves separated vertically (but otherwise identical to those in Figure 3) where the meridional advection of air parcels at the level of each CRW is felt higher up or lower down at the level of the other. All arrows are as in Figure 3. Taken from Heifetz *et al.* (2004a).

2.2 The CRW equations

With a physical picture of the interaction between two edge waves in place, we seek a set of equations to describe the evolution of their amplitudes and phases. We recall:

$$\frac{\partial q}{\partial t} + \bar{u}\frac{\partial q}{\partial x} + v\bar{q}_y = 0 \tag{35}$$

Following Heifetz *et al.* (2004a), we write the total PV perturbation q and the associated meridional wind v as linear combinations of the two CRW's:

$$q = Q_1 e^{i\epsilon_1} q_1 + Q_2 e^{i\epsilon_2} q_2 \tag{36}$$

$$v = Q_1 e^{i\epsilon_1} v_1 + Q_2 e^{i\epsilon_2} v_2 \tag{37}$$

where Q_1, Q_2 are the amplitudes of the two waves and ϵ_1, ϵ_2 are their phases. We assume wave-like perturbations in the zonal direction:

$$q_j = \tilde{q}_j e^{ikx} \qquad \psi_j = \tilde{\psi}_j e^{ikx} \tag{38}$$

Recalling $v = \frac{\partial \psi}{\partial x}$, we put:

$$v_j = -i\tilde{v}_j e^{ikx} = ik\tilde{\psi}_j e^{ikx} \tag{39}$$

At z_1, the location of wave 1, we must have $q_2 = 0$, i.e. the PV there is descibed purely by q_1. Substituting (36) and (37) into (35) with $q_2 = 0$ and, dividing by e^{ikx}, we obtain the evolution of amplitude and phase at z_1:

$$\left(\dot{Q}_1 e^{i\epsilon_1} + i\dot{\epsilon}_1 Q_1 e^{i\epsilon_1} + ik\bar{u}_1 Q_1 e^{i\epsilon_1} \right) \tilde{q}_1 - i \left(Q_1 e^{i\epsilon_1} \tilde{v}_1 + Q_2 e^{i\epsilon_2} \tilde{v}_2 \right) \bar{q}_{y1} = 0 \tag{40}$$

where dotted letters denote time derivatives and $\bar{u}_i$ and $\bar{q}_{yi}$ denote the velocity and PV gradient at the location of wave i. Dividing by $Q_1 e^{i\epsilon_1} \tilde{q}_1$ and equating the real and imaginary parts we obtain:

$$\dot{Q}_1 = -Q_2 \gamma_2^1 \sin\epsilon \tag{41}$$

$$\dot{\epsilon}_1 = -k\bar{u}_1 + \gamma_1^1 + \frac{Q_2}{Q_1}\gamma_2^1 \cos\epsilon \tag{42}$$

where $\epsilon = \epsilon_2 - \epsilon_1$ is the phase difference between the two waves and:

$$\gamma_j^i = \frac{\tilde{v}_j}{\tilde{q}_i}\bar{q}_{yi} \tag{43}$$

describes the effect of the meridional wind induced by wave j felt at wave i. Applying the same method at z_2, the location of wave 2, and thus imposing $q_1 = 0$, we obtain:

$$\dot{Q}_2 = Q_1 \gamma_1^2 \sin\epsilon \tag{44}$$

$$\dot{\epsilon}_2 = -k\bar{u}_2 + \gamma_2^2 + \frac{Q_1}{Q_2}\gamma_1^2 \cos\epsilon \tag{45}$$

Equations (41), (42), (44) and (45) are known as the CRW evolution equations. (41) and (44) demonstrate that the amplitude of each wave evolves purely due to interaction with the other wave. (42) and (45) demonstrate the evolution of the

phase speed of each wave is a combination of advection by the basic state zonal flow (the first term in each), its own natural propagation direction due to the sign of the PV gradient on which it is formed (the second term in each) and the effect of the other wave on its propagation direction (the third term of each). A further condition is required to completely specify the relative CRW amplitudes. Heifetz *et al.* (2004a) argue that the most appropriate one is:

$$-\gamma_2^1 = \gamma_1^2 = \gamma \tag{46}$$

where $\gamma > 0$ is known as the interaction coefficient. Equations (41), (42), (44) and (45) can then be simplified to:

$$\dot{\chi} = \gamma \left(1 - \chi^2\right) \sin\epsilon \tag{47}$$

$$\dot{\epsilon} = -k \left(c_2^2 - c_1^1\right) + \gamma \left(\chi + \frac{1}{\chi}\right) \cos\epsilon \tag{48}$$

where $\chi = \frac{Q_1}{Q_2}$ and $c_i^i = \bar{u}_i - \frac{\gamma_i^i}{k}$ is the phase speed of wave i in the absence of interacton (referred to as the *intrinsic* phase speed of wave i).

In the phase-locked configuration, the two waves must grow at the same rate. Therefore, from (41), (44) and (46), the normal mode growth rate, i.e. the rate of change of amplitude for both waves in the phase-locked configuration (the GNM or DNM), is given by:

$$\sigma = \gamma \sin\epsilon_{\mathrm{NM}} \tag{49}$$

where ϵ_{NM} is the normal mode phase difference. This illustrates that mutual growth occurs for $0 < \epsilon < \pi$ and mutual decay occurs for $-\pi < \epsilon < 0$ as argued in Section 2.1.

We now consider the GNM alone. From (41), (44) and (46), we see that when the two waves have equal growth rates (as per the GNM) they also have equal amplitudes. From (48), we see that equal phase speeds $\dot{\epsilon} = 0$ (as per the GNM) implies:

$$\cos\epsilon^+ = \frac{k(c_2^2 - c_1^1)}{2\gamma} \tag{50}$$

where ϵ^+ denotes the GNM phase difference. Combining (49) and (50) and using $\cos^2\phi + \sin^2\phi = 1$, we obtain:

$$\sigma = \left(\gamma^2 - \frac{k^2 \left(c_2^2 - c_1^1 \right)^2}{4} \right)^{\frac{1}{2}} \tag{51}$$

Given the dependence of wavelength on growth rate, we would thus like to discover the fastest growing wavelengths for specific basic states defined by $\bar{u}$ and $\bar{q}_y$. First however, it is necessary to describe how an expression for $\bar{q}_y$ is obtained.

2.3 Formulation of the PV gradient

From (30), assuming constant N, the basic state PV is given by:

$$\bar{q} = f_0 + \beta y + \frac{\partial^2 \psi}{\partial x^2} + \frac{\partial^2 \psi}{\partial y^2} + \frac{f_0^2}{N^2} \frac{1}{\rho} \frac{\partial}{\partial z} \left(\rho \frac{\partial \psi}{\partial z} \right) \tag{52}$$

As stated earlier, in stability studies, the basic state is taken to be zonally symmetric so that $\bar{u} = \bar{u}(y, z)$. We recall the horizontal wind equations:

$$\bar{v} = \frac{\partial \psi}{\partial x}, \quad \bar{u} = -\frac{\partial \psi}{\partial y} \tag{53}$$

Substituting (53) into (52), assuming no basic state meridional velocity $\bar{v} = 0$ and differentiating w.r.t. y, we obtain the basic state meridional PV gradient:

$$\bar{q}_y = \beta - \frac{\partial^2 \bar{u}}{\partial y^2} - \frac{f_0^2}{N^2} \frac{1}{\rho} \frac{\partial}{\partial z} \left(\rho \frac{\partial \bar{u}}{\partial z} \right) \tag{54}$$

For a purely baroclinic flow as we are interested in, i.e. $\bar{u}$ varies only in the vertical, (54) becomes:

$$\bar{q}_y = \beta - \frac{f_0^2}{N^2} \frac{1}{\rho} \frac{\partial}{\partial z} \left(\rho \frac{\partial \bar{u}}{\partial z} \right) \tag{55}$$

Substituting the exponentially decaying density profile (16) into (55), we obtain:

$$\bar{q}_y = \beta + \frac{f_0^2}{N^2} \left(\frac{1}{H_\rho} \frac{\partial \bar{u}}{\partial z} - \frac{\partial^2 \bar{u}}{\partial z^2} \right) \tag{56}$$

Using the Held height scale (7), we find that:

$$\bar{q}_y = \beta \left(1 + \frac{H_z}{H_\rho} \frac{\partial \hat{u}}{\partial \hat{z}} - \frac{\partial^2 \hat{u}}{\partial \hat{z}^2} \right) \tag{57}$$

16

meaning that $\bar{q}_y$ is non-dimensionalised with a scale of β. So, from (57), in order to satisfy the Charney-Stern criterion for baroclinic instability (33), we require a vertical zonal velocity profile $\hat{u}(\hat{z})$ such that $\frac{d^2\hat{u}}{d\hat{z}^2} - \frac{H_z}{H_\rho}\frac{d\hat{u}}{d\hat{z}} > 1$ somewhere in the vertical and $\frac{d^2\hat{u}}{d\hat{z}^2} - \frac{H_z}{H_\rho}\frac{d\hat{u}}{d\hat{z}} < 1$ somewhere else in the vertical.

2.4   The Charney model

The constant density Charney model describes the simplest basic state where baroclinic growth via CRW interaction is possible without an upper boundary. It consists of a negative potential temperature gradient at the ground $\theta_y < 0$ (as is normally the case in the Northern Hemisphere) in thermal wind balance with a uniform increase of zonal wind with height:

$$\bar{u} = \Lambda z \tag{58}$$

where Λ is a positive constant. For constant density, $H_\rho = \infty$ from (16). Also, from (58), $\frac{\partial^2 u}{\partial z^2} = 0$. Therefore, from (57), the PV gradient is equal to β, i.e. constant and positive. Note that, from (43), the evolution of amplitude is proportional to $\bar{q}_y$ so, from (57), we see that the introduction of density decay would increase $\bar{q}_y$ so that baroclinic growth would be faster.

So it may seem that, since there is no negative PV gradient, the Charney-Stern criterion (33) cannot be satisfied for the Charney model and so CRW's are not possible. However, we shall now see that, due to the negative PT gradient at the ground, a pair of CRW's can indeed be formed.

2.5   Boundary waves

We recall the equation for hydrostatic balance:

$$\frac{\partial \psi}{\partial z} = \frac{b'}{f_0} \tag{59}$$

For a warm anomaly ($b' > 0$), concentrated at the ground with no interior PV anomalies above it, (59) shows that the induced streamfunction ψ increases with height. Since we must have decay of the streamfunction with height, this means that $\psi < 0$ near the ground. Similarly, the streamfunction must decay with horizontal distance from the centre of the perturbation. From (22), this negative streamfunction is associated with a negative pressure anomaly. Therefore, there is cyclonic circulation (positive q) around the negative ψ anomaly and hence a positive tem-

perature anomaly behaves as a positive PV anomaly. By a reverse argument, a cold anomaly ($b' < 0$) induces an anti-cyclonic circulation around a positive streamfunction anomaly and so behaves as a negative PV anomaly.

Since, in the case of the Charney model, a negative temperature anomaly at the boundary induces anticyclonic flow like a negative PV anomaly in the interior, a surface buoyancy wave propagates along basic state PT contours in the same way as interior PV waves propagate along PV contours.

For interior temperature anomalies with the boundary sufficiently far away (as is the case in Figure 2), cyclonic anomalies are induced by positive PV anomalies where $\frac{\partial^2 \psi}{\partial z^2} > 0$ and therefore, from (59), not at a local maximum or minimum in b'. Therefore, the above argument is valid only for boundary waves.

With a picture of shear instability via the interaction of a boundary temperature wave and an interior wave in place, we can derive an interesting characteristic of the GNM in the Charney model by first establishing the intrinsic phase speeds of each wave:

2.5.1 Boundary wave phase speed

The linearised thermodynamic equation in terms of bouyancy is:

$$\left(\frac{\partial}{\partial t} + \bar{u} \frac{\partial}{\partial x} \right) b' + v \bar{b}_y = 0 \tag{60}$$

For a boundary wave, we impose that it has no interior PV:

$$q = \frac{\partial^2 \psi}{\partial x^2} + \frac{f_0^2}{N^2} \frac{\partial^2 \psi}{\partial z^2} = 0 \tag{61}$$

The perturbation streamfunction is therefore given by:

$$\psi = A e^{i(kx - \omega t)} e^{-Nkz/f_0} \tag{62}$$

for some constant A. We therefore have:

$$v = ikA e^{ikx} e^{i(kx - \omega t)} \qquad b' = -NkA e^{i(kx - \omega t)} e^{-Nkz/f_0} \tag{63}$$

Substituting (63) into (60):

$$c = \frac{\omega}{k} = \bar{u} - \frac{1}{Nk}\bar{b}_y \tag{64}$$

2.5.2 Interior wave phase speed

From the PV evolution equation (35), assuming a wave-like perturbation purely in the x-direction with wavenumber k and frequency ω:

$$q = \tilde{q}(z)e^{i(kx-\omega t)} \tag{65}$$

$$\psi = \tilde{\psi}(z)e^{i(kx-\omega t)} \tag{66}$$

and hence, from the geostrophic streamfunction identities:

$$v = \frac{\partial \psi}{\partial x} \qquad q = \nabla^2 \psi \tag{67}$$

where N and ρ are assumed constant for the purposes of illustration, we obtain:

$$q = -k^2 \tilde{\psi}e^{i(kx-\omega t)} \qquad v = ik\tilde{\psi}e^{i(kx-\omega t)} \tag{68}$$

Substituting (68) into (35) and dividing by $\tilde{\psi}e^{i(kx-\omega t)}$, we obtain the phase speed for a Rossby wave propagating on an interior PV gradient:

$$c = \frac{\omega}{k} = \bar{u} - \frac{1}{k^2}\bar{q}_y \tag{69}$$

2.6 Existing results for the Charney model

Comparing (64) and (69), we see that as wavelength increases (i.e. as k decreases), the intrinsic westward phase speed of wave 2 increases more rapidly than the intrinsic eastward phase speed of wave 1. The CRW's can therefore only phase-lock in a hindering configuration, which from Figure 4, means $\frac{\pi}{2} < \epsilon^+ < \pi$. At $\epsilon^+ = \pi$, from (49), the growth rate σ is zero and so for a sufficiently large wavelength there can be no normal mode growth. This is known as the first neutral point. Lindzen *et al.* (1980) have shown that the first neutral point for the Charney model occurs at:

$$r = \left(1 + \frac{2H_z}{H_\rho}\right)^{\frac{1}{2}} \tag{70}$$

which, for constant density, i.e. $H_\rho = \infty$, is equal to 1 as shown in Figure 6 where the dispersion relations for growth rate and phase speed are shown for the constant

density Charney model. We see neutral points at integer r where $r = \frac{\lambda}{4\pi L}$ is the non-dimensional wavelength. There is a maximum at $r \approx 0.63$. For mid-latitudes, f_0 is greater and β smaller than those given in Section 1.3 for westerly jets due to the latitude dependence. In this case Heifetz *et al.* (2004b) have used $f_0 = 10^{-4}\text{s}^{-1}$ and $\beta = 1.6 \times 10^{-11}\text{m}^{-1}\text{s}^{-1}$, which, using the expressions for scales given in Section 1.3, implies $H_z \approx 15\text{km}$, $L \approx 1650\text{km}$, $U \approx 45\text{ms}^{-1}$ and $T \approx 10$ hours. Since, in this case $r = 1$ corresponds to a wavelength of approximately 21,000 km, we are solely interested in the the region $0 < r < 1$ before the first neutral point.
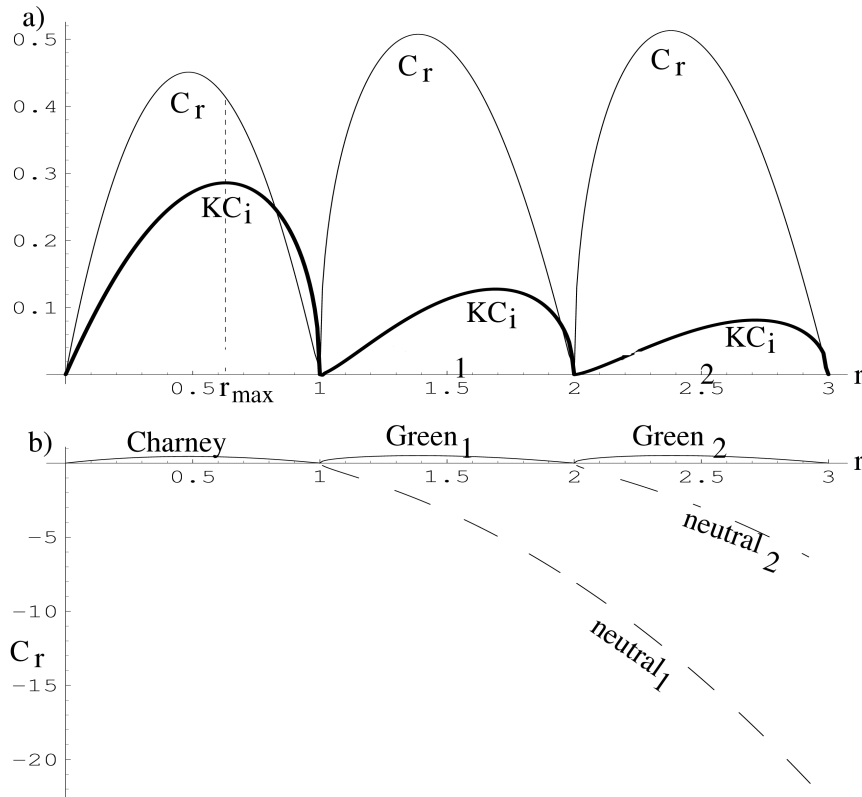

Figure 6: Dispersion relations for the normal modes in the constant density Charney model with non-dimensional wavelength r along the horizontal axis. (a) Eastward phase speed, denoted C_r and growth rate, denoted KC_i of the unstable modes. Neutral points occur at integer r. (b) Westward phase speed of the first two neutral modes shown with the eastward phase speeds of the unstable modes from (a). Note the change in scale from (a). Taken from Heifetz *et al.* (2004b)

In Figure 7, the PV structures and induced meridional wind structures are shown for each CRW in the constant density Charney model. We see that, as required, the upper CRW has zero PV at the ground where the lower CRW has a PV maximum and the lower CRW has zero PV at the level where the upper wave has a PV
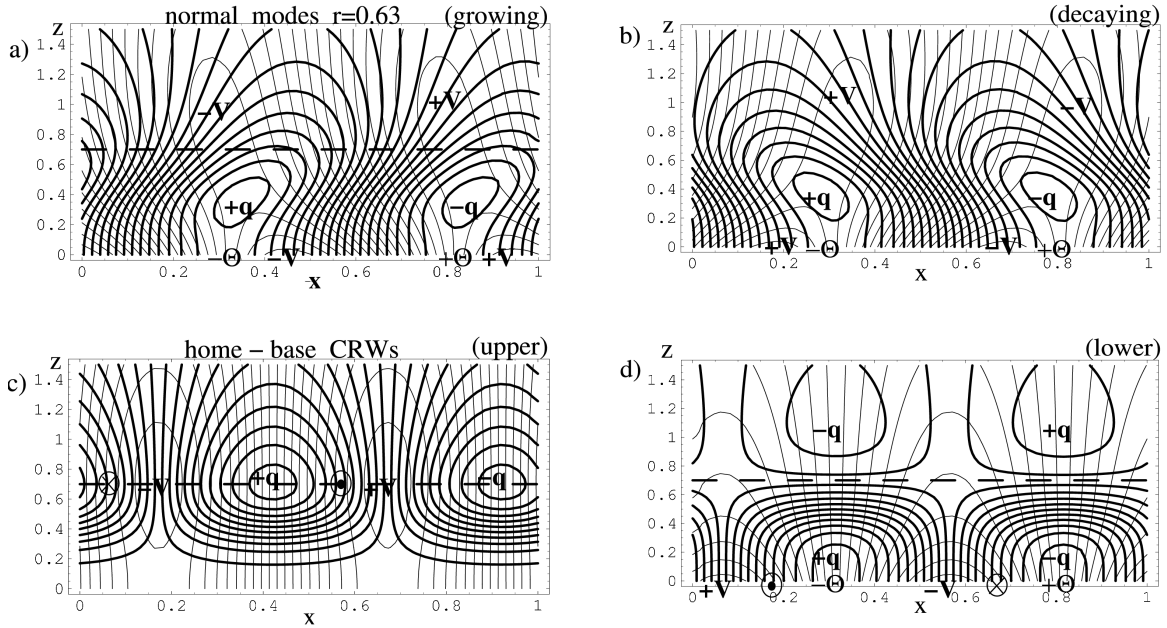
Figure 7: Non-dimensionalised x-z cross sections showing contours of PV q **and induced meridional wind** v in the constant density Charney model. Surface PT anomalies are also indicated by Θ. The positive and negative meridional wind that each CRW induces at the other's home-base is denoted by circled crosses and dots respectively. (a) The fastest growing normal mode (as obtained in 6). (b) The corresponding DNM, defined as the complex conjugate as the GNM in (a). (c) and (d) The upper and lower CRW's obtained using the home-base method. Taken from Heifetz *et al.* (2004b)

maximum. Since the upper CRW has no temperature anomaly at the ground, its induced flow is simply cyclonic (anti-cyclonic) around the positive (negative) PV anomalies. Regarding the lower CRW, we note that, since at the ground $\theta_y < 0$ but $\bar{q}_y = \beta > 0$, northward displacement of air parcels implies a *positive* PT anomaly but a *negative* PV anomaly (see Figure 2) with the reverse true for a southward displacement. Therefore, since the lower CRW is defined by a strong temperature anomaly signature which overwhelms the interior PV, the induced flow is cyclonic (anti-cyclonic) around the positive (negative) temperature anomalies, despite the negative (positive) interior PV there. This leads to the eastward tilt in PV contours but westward tilt in meridional wind contours that we see for the GNM (where $\epsilon > 0$), with the reverse true for the DNM. In Figure 8, CRW structures for the constant density Charney model are shown. For the upper CRW we see a positive PV anomaly structure with the greatest maximum amplitude obtained for $r = 0.63$, shown to be the fastest GNM in Figure 6. The PV structure tends to exponential

21
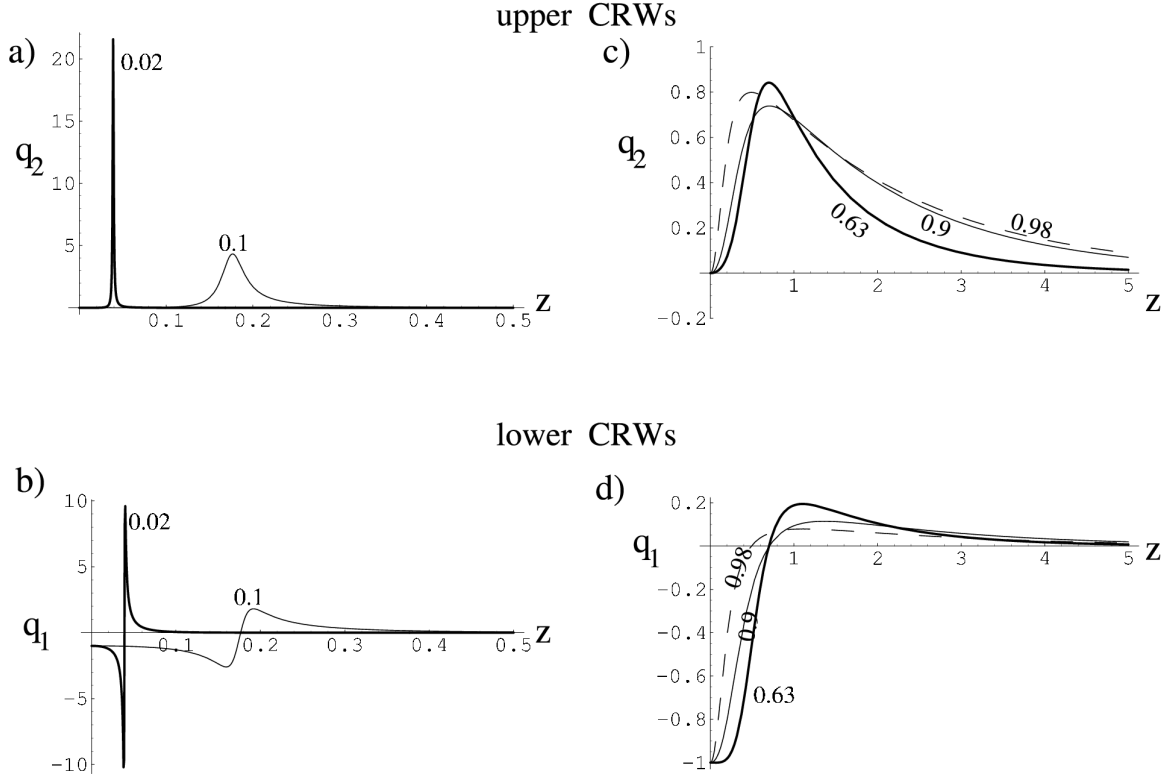
Figure 8: Vertical PV structures of the upper and lower CRW's obtained using the home-base method in the constant density Charney model. Amplitudes are normalised so that, when superposed with the correct phase difference, they reconstruct the GNM normalised by its surface tempertature. The numbers label the wavelengths r. (a) and (b) show the upper CRW and (c) and (d) the lower CRW. Taken from Heifetz *et al.* (2004b).

decay from the ground as $r \to 1$ and tends to a δ function at the ground as $r \to 0$. The fastest GNM has its homebase the furthest from the ground. The lower CRW has negative PV at the ground, extending as far as the boundary PT anomalies are able to overwhelm the interior PV anomalies.

Having observed some of the CRW's and PV structures that have been found for westerly jets in the literature, we now wish to establish these for easterly jets. First though a model description is needed.

3 Semi-analytic model procedure

3.1 Outline of problem

As stated in the introduction we wish to look at the time evolution of PV perturbations on the AEJ in order to address each of the questions posed and compare AEW characteristics to the characteristics of waves propagating on westerly jets in the literature. We therefore require a model that will take an initial PV perturbation $q_0(x, z)$ and allow it to develop according to the linearised PV conservation equation (35).

$$\frac{\partial q}{\partial t} + \bar{u}\frac{\partial q}{\partial x} + v\bar{q}_y = 0 \tag{71}$$

for a given basic state. We use a semi-analytic model as developed by Hylke De Vries for his thesis (De Vries (2006)) and used by Methven and de Vries (2008) to perform basic experiments for the time evolution of simple initial PV structures on a basic state defined by a uniform westerly shear. The use of the model to simulate PV evolution on the AEJ consists merely of altering the basic state zonal flow definition. The model works as follows:

Assuming wavelike perturbations in the x-direction, the perturbation streamfunction and PV are written:

$$\psi(x, z, t) = e^{ikx}\tilde{\psi}(z, t) \tag{72}$$

$$q(x, z, t) = e^{ikx}\tilde{q}(z, t) \tag{73}$$

Substituting (72) and (73) into (71) and dividing by e^{ikx}, we obtain:

$$\frac{\partial \tilde{q}}{\partial t} = -ik\left(\bar{u}\tilde{q} + \bar{q}_y\tilde{\psi}\right) \tag{74}$$

For a given basic state, i.e. where $\bar{q}_y$ and $\bar{u}$ are known functions of z, we seek a solution to (74) in terms of a perturbation defined by $\tilde{q}$ and $\tilde{\psi}$. From (74), we see that, if we know the PV and streamfunction at a given time, then we can find the PV at a subsequent time. Thus for an initial value problem, where the initial PV structure is defined, we seek a means of obtaining the streamfunction from the PV at a given time. From (30), for constant N, the instantaneous PV *perturbation* is related to the corresponding streamfunction as follows:

$$q(x, y, z) = \frac{\partial^2 \psi}{\partial x^2} + \frac{\partial^2 \psi}{\partial y^2} + \frac{f_0^2}{N^2}\frac{1}{\rho}\frac{\partial}{\partial z}\left(\rho\frac{\partial \psi}{\partial z}\right) \tag{75}$$

(75) states that the perturbation PV is equal to the curvature of the perturbation streamfunction. For a flow perturbed in the x-z plane alone, (75) can be simplified to:

$$q(x, \hat{z}) = \frac{\partial^2 \psi}{\partial x^2} + \frac{1}{\rho} \frac{\partial}{\partial \hat{z}} \left(\rho \frac{\partial \psi}{\partial \hat{z}} \right) \tag{76}$$

where $\hat{z} = \frac{N}{f_0} z$. Note, since N and f_0 have the same dimensions, $\hat{z}$ is not non-dimensional, just rescaled, and is different to the non-dimensional $\hat{z}$ introduced in Section 1.3. We hereafter dispense with the circumflex (^) notation for the remainder of this section so that z refers to height rescaled by $\frac{N}{f_0}$ until further notice. From (72) and (76), we have:

$$\tilde{q}(z) = -k^2 \tilde{\psi}(z) + \frac{1}{\rho} \frac{d}{dz} \left(\rho \frac{d\tilde{\psi}}{dz} \right) \tag{77}$$

Thus we seek a means of inverting the differential operator in (77). One way of doing so is to consider the corresponding Green function problem:

$$-k^2 G(z, h) + \frac{1}{\rho} \frac{d}{dz} \left(\rho \frac{dG}{dz} \right) = \delta(z - h) \tag{78}$$

where the RHS is zero for $z \neq h$ and, by Green function theory:

$$\tilde{q}(z) = \int_0^\infty \delta(z - h) \tilde{q}(h) dh \tag{79}$$

$$\tilde{\psi}(z) = \int_0^\infty G(z, h) \tilde{q}(h) dh \tag{80}$$

From (79), the PV at z is the integral over all vertical levels $h \geq 0$ of the PV at h multiplied by the $\delta(z - h)$ function. The δ function therefore ensures that only the PV at $h = z$ contributes to $\tilde{q}(z)$ at a given instant (as is logically necessary). From (80), however, we see that, due to the Green function $G(z, h)$, the PV at *every* level $h \geq 0$ contributes to the streamfunction at z.

The physical interpretation of this is to consider the PV at each vertical level to be a δ function spike which is concentrated into a single infinitesimal layer. However, due to the advection of air parcels that it excites, it is contributing at any given instant to the streamfunction at all other levels. Where the basic state meridional PV gradient is non-zero, the induced meridional wind will advect PV and hence modify PV anomalies. Following Heifetz and Methven (2005), we call the stream-

24

function associated with a PV spike at $z = h$ a **Kernel Rossby Wave** (KRW) at h and say that the KRW at h excites the KRW's at all other levels z.

In order to represent (74) in a numerical model, we discretise the vertical into N strips of width Δz so that z is defined at $z_0, z_1, \ldots, z_N$ where $z_j = j\Delta z$. Representing the time derivative in (74) by a finite difference approximation, we can find that $\tilde{q}^{n+1}$, the x-independent part of the PV at time t^{n+1}, can be obtained if we know both $\tilde{q}^n$ and $\tilde{\psi}^n$. Thus for an initial value problem, where $\tilde{q}_j^0 = \tilde{q}^0(z_j)$ is given for $j = 0, 1, \ldots, N$, we obtain the streamfunction $\tilde{\psi}^n$ from the PV $\tilde{q}^n$ at each time t^n for $n = 0, 1, 2, \ldots$ using the Green function method.

We consider a KRW at each level $z_0, z_1, \ldots, z_N$. In reality, there are an infinite number of KRW's throughout the vertical, each representing the PV at a given level. Therefore as $\Delta z \to 0$ and hence $N \to \infty$, the model approaches the continuous flow.

$G(z, h)$ represents the streamfunction associated with the PV δ function at $z = h$ and its role is to determine the extent to which the KRW at h affects the streamfunction at z. So, from (80), the total streamfunction at a given level is the sum of the streamfunction contributions of each KRW. So we expect the Green function to peak at $z = h$ (i.e. affect the streamfunction at its own level the most) and fall either side, the further from $z = h$ its effect is felt. We thus turn our attention to the structure of the Green functions in question.

3.2 Specific Green functions

We recall:

$$-k^2 G(z, h) + \frac{1}{\rho}\frac{d}{dz}\left(\rho\frac{dG}{dz}\right) = \delta(z - h) \tag{81}$$

The exact Green function therefore is obtained as a solution to the homogenous problem (with the RHS equal to zero) for two subdomains either side of the delta-function at $z = h$. The exact solution depends on a choice of boundary conditions and density profile.

In order to establish a boundary condition for G, we recall the equation for hydrostatic balance:

$$b' = f_0\frac{\partial\psi}{\partial z} \tag{82}$$

Assuming no potential temperature perturbation at the boundary, $\theta' = 0$ and hence $b' = \frac{g\theta'}{\theta_0} = 0$, we obtain:

$$\frac{d\tilde{\psi}}{dz} = 0 \tag{83}$$

Hence, from (80) :

$$\frac{dG}{dz} = 0 \qquad \text{at solid boundaries} \tag{84}$$

In the absence of an upper boundary, we require that the effect of a KRW at $z = h$ decays to zero as the distance from h tends to infinity. Thus:

$$G \to 0 \quad \text{as } z \to \infty \qquad \text{if no upper boundary} \tag{85}$$

We now find three specific Green functions for different density and boundary specifications.

3.2.1 Constant density with a rigid lid

We first find the Green function, G_1, for the case where z is bounded at $z = H$ (as well as at $z = 0$) and the density is constant.

For constant ρ, (78) becomes:

$$\frac{d^2G}{dz^2} - k^2G = \delta(z - h) \tag{86}$$

Thus we require exponential solutions. Imposing boundaries at $z = 0, H$, we require $\frac{dG}{dz} = 0$ at these heights. In order to satisfy both these conditions we must construct a solution consisting of two separate branches. From (86), there must be a discontinuity in the gradient at $z = h$ so this is the point where the two branches must meet (which confirms the notion that the Green function should have a maximum at $z = h$, i.e. a KRW should have the greatest effect at its own level). Thus the general solution is:

$$G_1(z, h) = \begin{cases} A\cosh\left[k\left(H - z\right)\right] & z > h \\ B\cosh(kz) & z < h \end{cases} \tag{87}$$

For continuity we require that the two branches of the solution meet at $z = h$:

$$A\cosh\left[k\left(H - h\right)\right] = B\cosh(kh) \tag{88}$$

We can obtain a further condition on the solution by considering the discontinuity in $\frac{dG}{dz}$ at $z = h$ that the δ function creates. Integrating (86) between $h - \Delta z$ and $h + \Delta z$:

$$\int_{h-\Delta z}^{h+\Delta z} \frac{d^2 G}{dz^2} dz - k^2 \int_{h-\Delta z}^{h+\Delta z} G dz = \int_{h-\Delta z}^{h+\Delta z} \delta(z - h) dz \tag{89}$$

we obtain:

$$\left[\frac{dG}{dz}\right]_{h-\Delta z}^{h+\Delta z} - k^2 \int_{h-\Delta z}^{h+\Delta z} G dz = 1 \tag{90}$$

using the fundamental property of the δ function. As $\Delta z \to 0$, the area under the G curve between $h - \Delta z$ and $h + \Delta z$ must tend to zero since G is everywhere finite. Hence the second term on the LHS of (90) disappears. However, due to the aforementioned discontinuity in $\frac{dG}{dz}$ at $z = h$, the first term remains, leaving:

$$\left[\frac{dG}{dz}\right]_{h-\Delta z}^{h+\Delta z} \to 1 \quad \text{as } \Delta z \to 0 \tag{91}$$

meaning that there is a change of 1 in $\frac{dG}{dz}$ at $z = h$, indicating a minimum in G at $z = h$ (but still a maximum of the modulus since a KRW at $z = h$ should have the greatest effect at its own level). Applying (91) to (87) yields:

$$-kA\sinh\left[k\left(H - h\right)\right] - kB\sinh(kh) = 1 \tag{92}$$

Substituting (88) into (92) we obtain:

$$kA\sinh\left[k\left(H - h\right)\right] + \frac{kA\sinh\left(kh\right)\cosh\left[k\left(H - h\right)\right]}{\cosh(kh)} = -1 \tag{93}$$

Hence we deduce:

$$A = -\frac{\cosh(kh)}{k\left[\cosh(kh)\sinh\left[k\left(H - h\right)\right] + \sinh(kh)\cosh\left[k\left(H - h\right)\right]\right]} \tag{94}$$

which, using the identity $\sinh\left(\phi_1 + \phi_2\right) = \cosh\phi_1\sinh\phi_2 + \sinh\phi_1\cosh\phi_2$, simplifies to:

$$A = -\frac{\cosh(kh)}{k\sinh(kH)} \tag{95}$$

and hence, substituting (95) into (88):

$$B = -\frac{\cosh\left[k\left(H - h\right)\right]}{k\sinh(kH)} \tag{96}$$

giving the full solution:

$$G_1(z, h) = -\frac{1}{k\sinh(kH)} \begin{cases} \cosh(kh)\cosh\left[k\left(H-z\right)\right] & z > h \\ \cosh\left[k\left(H-h\right)\right]\cosh(kz) & z < h \end{cases} \tag{97}$$

3.2.2 Constant density without a rigid lid

We now seek the Green function, G_2, for the model with no upper boundary but still constant density. We now require $\frac{dG}{dz} = 0$ at $z = 0$ and $G \to 0$ as $z \to \infty$. From (86), this implies that the full solution should be as follows:

$$G_2(z, h) = \begin{cases} Ae^{-k(z-h)} & z > h \\ B\cosh(kz) & z < h \end{cases} \tag{98}$$

The ODE for G_2 is the same as for G_1 so (91) is also valid in this case. Therefore the conditions at $z = h$ of continuity and unit change in $\frac{dG}{dz}$ yield, respectively:

$$A = B\cosh(kh) \tag{99}$$

$$-kA - kB\sinh(kh) = 1 \tag{100}$$

Combining (99) and (100), we obtain:

$$B\left(\cosh(kh) + \sinh(kh)\right) = -\frac{1}{k} \tag{101}$$

Hence:

$$B = -\frac{1}{k}e^{-kh} \tag{102}$$

Hence, substituting (102) into (99):

$$A = -\frac{1}{2k}\left(1 + e^{-2kh}\right) \tag{103}$$

Thus the full solution is given by:

$$G_2(z, h) = -\frac{1}{2k} \begin{cases} \left(1 + e^{-2kh}\right)e^{-k(z-h)} & z > h \\ 2e^{-kh}\cosh(kz) & z < h \end{cases} \tag{104}$$

3.2.3 Exponentially decaying density without a rigid lid

Finally, we find the Green function, G_3, where there is no rigid lid and we vary the density field to decay with height as is observed to be a good approximation

in the atmosphere due to its compressibility and approximate hydrostatic balance (17). Putting:

$$\rho(z) = \rho_0 e^{-z/H_\rho} \tag{105}$$

and substituting into (78) we obtain:

$$-k^2 G + e^{z/H_\rho} \frac{d}{dz}\left(e^{-z/H_\rho}\frac{dG}{dz}\right) = \delta(z-h) \tag{106}$$

Hence:

$$\frac{d^2 G}{dz^2} - \frac{1}{H_\rho}\frac{dG}{dz} - k^2 G = \delta(z-h) \tag{107}$$

By considering the corresponding quadratic characteristic equation for this ODE, this gives the general solution:

$$G_3(z,h) = \begin{cases} A\left(C_1 e^{\lambda_1(z-h)} + D_1 e^{\lambda_2(z-h)}\right) & z > h \\ B\left(C_2 e^{\lambda_1 z} + D_2 e^{\lambda_2 z}\right) & z < h \end{cases} \tag{108}$$

where $\lambda_{1,2} = \frac{1 \pm \sqrt{1+4k^2 H_\rho^2}}{2H_\rho}$. Again, we require $G \to 0$ as $z \to \infty$. This implies $C_1 = 0$ since $\lambda_1 > 0$ and $\lambda_2 < 0 \; \forall k > 0$.

Again, we also require $\frac{dG}{dz} = 0$ at $z = 0$. This implies $\lambda_1 C_2 + \lambda_2 D_2 = 0$ and so $D_2 = -\frac{\lambda_1}{\lambda_2} C_2$.

Thus, allowing A to absorb D_1 and B to absorb $\frac{C_2}{\lambda_2}$, we obtain:

$$G(z,h) = \begin{cases} A e^{\lambda_2(z-h)} & z > h \\ B\left(\lambda_2 e^{\lambda_1 z} - \lambda_1 e^{\lambda_2 z}\right) & z < h \end{cases} \tag{109}$$

Since the ODE for G_3 is different to that for G_1 and G_2, we must check that the condition of unit change in $\frac{dG}{dz}$ at $z = h$ is still valid. Integrating (107) between $h - \Delta z$ and $h + \Delta z$:

$$\left[\frac{dG}{dz}\right]_{h-\Delta z}^{h+\Delta z} - \frac{1}{H_\rho}[G]_{h-\Delta z}^{h+\Delta z} - k^2 \int_{h-\Delta z}^{h+\Delta z} G \, dz = 1 \tag{110}$$

As $\Delta z \to 0$, the change in G between $h - \Delta z$ and $h + \Delta z$ must tend to zero, since G is continuous. Therefore the second term on the LHS of (110) disappears (as, it has already been demonstrated, does the third term) and so (91) is indeed valid in this case also. Therefore the conditions at $z = h$ of continuity and unit change in

29

$\frac{dG}{dz}$ yield, respectively:

$$A = B \left(\lambda_2 e^{\lambda_1 h} - \lambda_1 e^{\lambda_2 h} \right) \tag{111}$$

$$\lambda_2 A - \lambda_1 \lambda_2 B \left(e^{\lambda_1 h} - e^{\lambda_2 h} \right) = 1 \tag{112}$$

Substituting (111) into (112):

$$\lambda_2 B \left(\lambda_2 e^{\lambda_1 h} - \lambda_1 e^{\lambda_2 h} \right) - \lambda_1 \lambda_2 B \left(e^{\lambda_1 h} - e^{\lambda_2 h} \right) = 1 \tag{113}$$

Hence:

$$B = \frac{1}{\lambda_2 \left(\lambda_2 - \lambda_1 \right)} e^{-\lambda_1 h} \tag{114}$$

And substituting (114) into (111):

$$A = \frac{1}{\lambda_2 - \lambda_1} \left(1 - \frac{\lambda_1}{\lambda_2} e^{(\lambda_2 - \lambda_1)h} \right) \tag{115}$$

giving the general solution:

$$G_3(z, h) = \frac{1}{\lambda_2 - \lambda_1} \begin{cases} \left(1 - \frac{\lambda_1}{\lambda_2} e^{(\lambda_2 - \lambda_1)h} \right) e^{\lambda_2(z-h)} & z > h \\ \frac{1}{\lambda_2} e^{-\lambda_1 h} \left(\lambda_2 e^{\lambda_1 z} - \lambda_1 e^{\lambda_2 z} \right) & z < h \end{cases} \tag{116}$$

3.3   Comparing Green functions

In reality, we have a density profile that decays with height and, although the tropopause can act as a rigid lid, the AEJ's mean height is approximately 4km (a quarter the height of the tropopause over West Africa), so G_3 is in fact the most realistic Green function and the one that will be used for all model simulations in this study. However, it is useful to plot all 3 together to illustrate the effects of unbounded flow and density decay on the Green function.

In Figure 9, G_1, G_2 and G_3 are plotted against z for $0 \leq z \leq H$ for $H = 10$km (where, in the case of G_1, H also represents the rigid lid). We put $H_\rho = 7$km and, following De Vries et $al.$ (2009), $k = \frac{1.6}{H}$ and vary the KRW height h. For all the curves shown, we see a smooth decrease above and below the height h of the KRW. This represents the streamfunction associated with a PV δ function at $z = h$ with decreasing effect on KRW's the further they are from $z = h$.
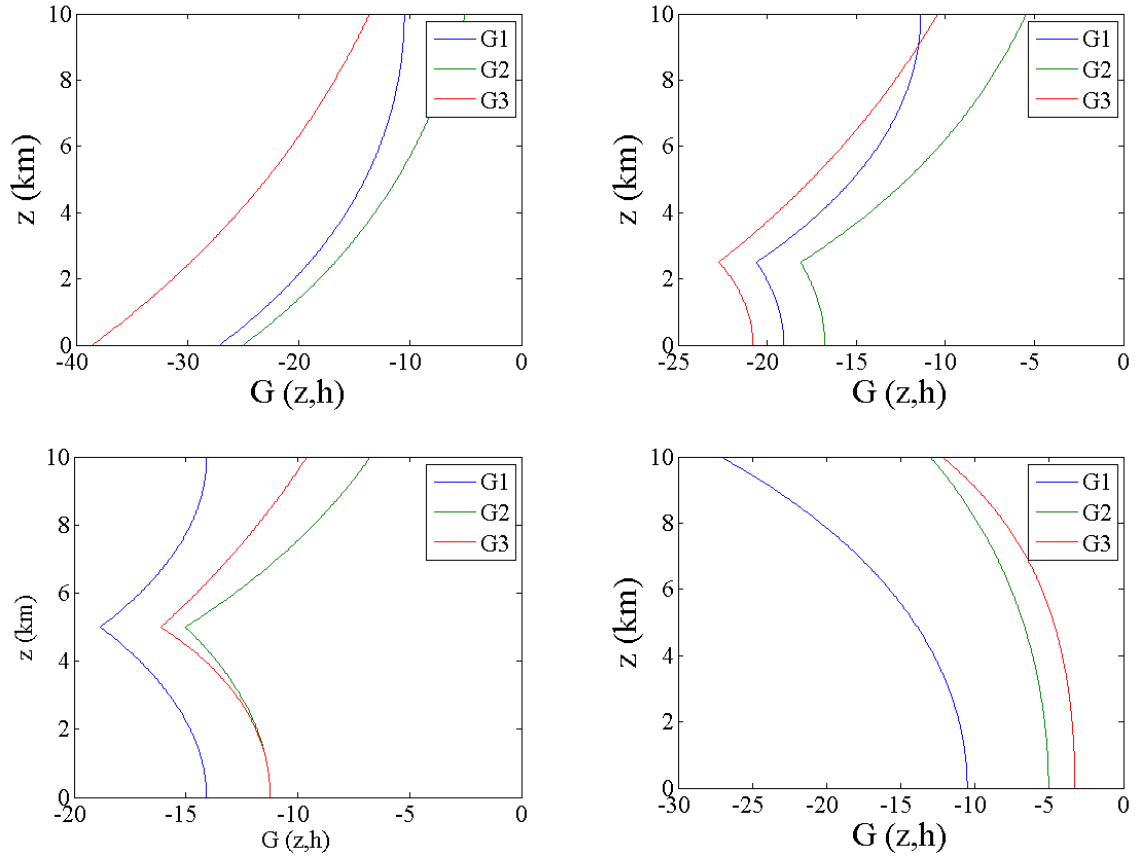
Figure 9: $G_1(z,h)$,$G_2(z,h)$ and $G_3(z,h)$ against (re-dimensionalised) z for $0 \leq z \leq$ 10 km with $H_\rho = 7$km and $k = 1.6 \times 10^{-4}$ m^{-1}. $h = 0$ (top left), 2.5 km (top right), 5 km (bottom left) and 10km (bottom right).

G_1 has greater amplitude than G_2 throughout the vertical in each figure. This illustrates the fact that, when a rigid lid is imposed, the effect of meridional advection felt higher up or lower down is magnified within the confined region.

For the KRW at the ground, G_3 (where the density decays with height) has greater magnitude throughout the vertical than G_2 (which is for an otherwise identical model). As we raise the level of the KRW, G_3 comes to have a smaller amplitude than G_2. This indicates that a KRW in an area of high density has a greater effect on a KRW in an area of lower density than if the density were constant.

3.4 Time evolution

Having established the exact Green functions for each model settings, we can simply evaluate them at each level z_j and incorporate the values obtained into the program as follows:

Substituting (79) and (80) into (74) and dividing by e^{ikx} we obtain:

$$\frac{\partial \tilde{q}}{\partial t} = -ik \left[\bar{u} \int_0^\infty \delta(z-h)\tilde{q}(h)dh + \frac{\partial q}{\partial y} \int_0^\infty G(z,h)\tilde{q}(h)dh \right] \tag{117}$$

where $\tilde{q}(h)$ is shorthand for $\tilde{q}(h,t)$. The RHS of (117) is known as the *linear dynamical operator* for $\tilde{q}$ and describes the evolution of PV using the Green function method. From (73) and (72) we see that z and t act to define the amplitude and phase of the waves that form along the x-axis. Hence, following Heifetz and Methven (2005), we put:

$$\tilde{q}(z,t) = Q(z,t)e^{i\epsilon(z,t)} \tag{118}$$

where $Q(z,t)$ and $\epsilon(z,t)$ are the amplitude and phase respectively of $q(x,z,t)$. We subsequently use the shorthand $Q(z)$ and $\epsilon(z)$. Substituting (118) into (117) and dividing by $e^{i\epsilon(z)}$, we obtain:

$$\dot{Q}+iQ(z)\dot{\epsilon} = -ik \left[\bar{u} \int_0^\infty Q(h)e^{i[\epsilon(h)-\epsilon(z)]}\delta(z-h)dh + \bar{q}_y \int_0^\infty Q(h)e^{i[\epsilon(h)-\epsilon(z)]}G(z,h)dh \right] \tag{119}$$

Finally, equating the real and imaginary parts of (119) and using the following identities:

$$\int_0^\infty f(h)\sin\left[\epsilon(z) - \epsilon(h)\right]\delta(z-h)dh = 0 \tag{120}$$

$$\int_0^\infty f(h)\cos\left[\epsilon(z) - \epsilon(h)\right]\delta(z-h)dh = 1 \tag{121}$$

we obtain the KRW amplitude and phase evolution equations:

$$\dot{Q} = -k\bar{q}_y \int_0^\infty Q(h)\sin\left[\epsilon(z) - \epsilon(h)\right]G(z,h)dh \tag{122}$$

$$\dot{\epsilon} = -k \left[\bar{u} + \bar{q}_y \int_0^\infty \frac{Q(h)}{Q(z)}\cos\left[\epsilon(z) - \epsilon(h)\right]G(z,h)dh \right] \tag{123}$$

(122) and (123) indicate that the amplitude and phase of each KRW evolves according to meridional displacements of air due to KRW's at every other level. The $G(z,h)$ function serves to magnify/reduce the effect of each KRW, depending on its

proximity to the KRW in question.

The leapfrog finite difference numerical scheme which we use to approximate the PV conservation equation (71) is thus:

$$\frac{Q_j^{n+1} - Q_j^{n-1}}{2\Delta t} = -k\Delta z \; \bar{q}_y(z_j) \sum_{i=0}^{N} \left(Q_i^n \sin\left(\epsilon_j^n - \epsilon_i^n\right) G(z_j, z_i) \right) \tag{124}$$

$$\frac{\epsilon_j^{n+1} - \epsilon_j^{n-1}}{2\Delta t} = -k \left[\bar{u}(z_j) + \Delta z \; \bar{q}_y(z_j) \sum_{i=0}^{N} \left(\frac{Q_i^n}{Q_j^n}\cos\left(\epsilon_j^n - \epsilon_i^n\right) G(z_j, z_i) \right) \right] \tag{125}$$

i.e. we use the amplitude and phase of the KRW's at all vertical levels $z_0, z_1, ..., z_N$ at time t^n as well as the known analytic functions $\bar{u}(z_j)$, $\bar{q}_y(z_j)$ and $G(z_j, z_i)$, in order to calculate the amplitude and phase of the KRW at z_j at time t^{n+1}. As such it is a semi-analytic model.

(122) and (123) describe the evolution of the *continuous spectrum* of PV. They can be constrasted with the simple CRW equations (41), (42), (44) and (45) where the evolution of PV is described by the interaction of 2 waves alone and hence known as the *discrete spectrum*. For a given initial perturbation, the CRW equations do not describe the full flow evolution as we shall see. In the subsequent sections we will use the KRW model described here to model the growth of perturbations on the AEJ and then establish how much of the growth can be explained by two CRW's. First, however, as stated at the beginning of this section, a definition of the basic state for the AEJ is required.

4 Defining idealised easterly jets and their stability

4.1 Derivation of basic state for easterly jet

With a model defined for the evolution of PV in terms of KRW phase and amplitude, we must establish a basic state for the AEJ defined by vertical profiles of zonal velocity $\bar{u}(z)$ and meridional PV gradient $\bar{q}_y$. These functions of z can then be substituted into the model equations (122) and (123) and will determine the instability of the jet. As discussed in Section 1.1, $\theta_y > 0$ at the ground ($z = 0$) in the region of the AEJ so baroclinic instability can be achieved by a negative $\bar{q}_y$ at some height in the interior, i.e. at some $z > 0$.

With a single well-defined scale established (see Section 1.3), we dispense with the circumflex (^) notation so that z,u hereafter denote the *non-dimensional* height and basic state zonal velocity respectively unless otherwise stated. Correspondingly, we hereafter use the notation for the dimensional PV gradient to denote the *non-dimensional* PV gradient, recalling (57):

$$\bar{q}_y = 1 + \frac{H_z}{H_\rho}\frac{du}{dz} - \frac{d^2u}{dz^2} \tag{126}$$

In a jet stream region, we expect to see a smooth vertical structure consisting of (i) a peak velocity at the jet core, (ii) near zero velocity at the boundary(ies) and (iii) a decay to zero as $z \to \infty$ if there is no upper boundary.

For the AEJ, we have just one boundary at $z = 0$. Therefore we put $u(z) = 0$ at $z = 0$ and $u(z) \to 0$ as $z \to \infty$.

One simple smooth function satisfying the given requirements is

$$u(z) = \tau z e^{-z/\gamma} \tag{127}$$

where the τ and γ parameters are inserted to allow us to define a jet that is appropriately scaled and centred. Hence:

$$\frac{du}{dz} = \tau e^{-z/\gamma}\left(1 - \frac{z}{\gamma}\right) \tag{128}$$

34

The observed mean height of the AEJ is 4 km. Hence, recalling the height scale $H_z = 2.2$km, we require u to have a maximum at $z = \frac{4}{2.2} = 1.8$. From (128), this maximum is given by $z_{jet} = \gamma$. Hence:

$$\gamma = 1.8 \tag{129}$$

The observed velocity of the AEJ core is -12 ms^{-1} (negative because of the easterly jet). Hence, recalling the velocity scale $U = 6.6$ms^{-1}, we require the maximum u to be $u_{jet} = \frac{-12}{6.6} = -1.8$. Hence, from (127), we obtain:

$$\tau = \frac{u_{jet}}{z_{jet}} e^{z_{jet}/\gamma} = -e \tag{130}$$

given that $\gamma = z_{jet}$ and $u_{jet} = -z_{jet}$. Hence, substituting (129) and (130) into (127), we obtain the exact solution for the vertical zonal wind profile that we will use to represent the AEJ:

$$u(z) = -ze^{\left(1 - \frac{z}{z_{jet}}\right)} \text{ where } z_{jet} = 1.8 \tag{131}$$

The fact that $|u_{jet}|$ and $|z_{jet}|$ are equal results from using $\Lambda = 3 \times 10^{-3}$s^{-1} which is in fact equal to $\frac{12\text{ms}^{-1}}{4000\text{m}}$, i.e. the dimensional jet velocity divided by the dimensional jet height. Hence $|\frac{u_{jetdim}}{U}| = |\frac{z_{jetdim}}{H_z}|$, where u_{jetdim} and z_{jetdim} refer to the dimensional values of u and z at the jet core.

Substituting (131) into (126), we obtain the meridional PV gradient as a function of z:

$$\bar{q}_y(z) = 1 - e^{\left(1 - \frac{z}{z_{jet}}\right)} \left[\frac{H_z}{H_\rho}\left(1 - \frac{z}{z_{jet}}\right) + \frac{2}{z_{jet}} - \frac{z}{z_{jet}^2}\right] \tag{132}$$

Figure 10 shows the zonal velocity and PV gradient through the vertical, using a density height scale of $H_\rho = 7.7$km. As we can see, $\bar{q}_y$ is positive at the ground (due to $\theta_y > 0$) but negative for approximately $0 < z < 1.5$, due to the curvature of the jet cancelling β. So the Charney-Stern criterion for instability is satisfied. Further, $u(0)$ is more negative where $q_y < 0$ than $u(z)$ where $q_y > 0$. Thus the Fjortoft criterion for instability is also satisfied. Hence if one CRW is formed at the ground and another somewhere between the ground and $z = 1.5$ then baroclinic growth can occur. It should be noted that, although q_y changes sign in the interior, thus satisfying the Charney-Stern criterion (33) there (independently of the boundary

temperature gradient), the basic state flow is greater (less negative) at the negative PV gradient (below $z = 1.5$) than at the positive PV gradient above, so the Fjortoft criterion (34) is not satisfied. Thus any anomalies created above $z = 1.5$ cannot lead to phase-locking CRW's.
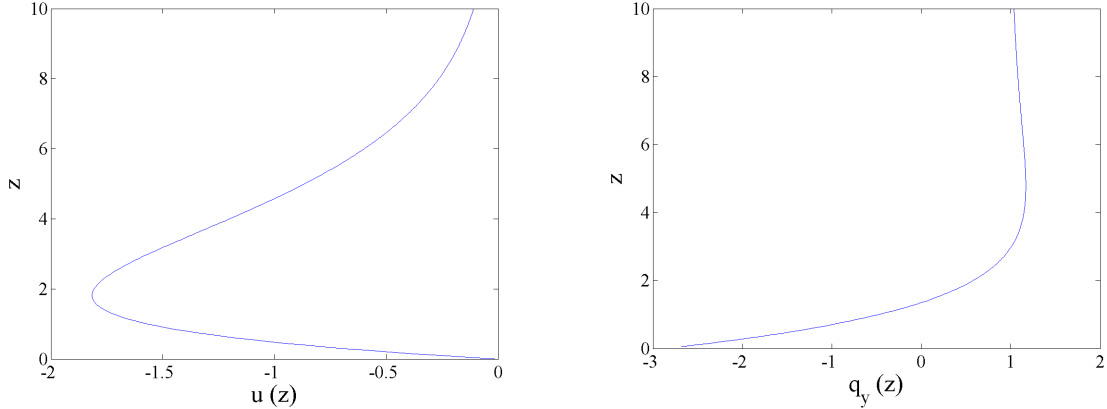

Figure 10: Basic state zonal velocity (left) and PV gradient (right) against height height for an easterly jet. All variables non-dimensional

4.2 Asymmetry between easterly and westerly jets

For the equivalent westerly jet we have, from (131):

$$u(z) = ze^{\left(1 - \frac{z}{z_{jet}}\right)} \text{ where } z_{jet} = 1.8 \tag{133}$$

and hence, substituting (133) into (57):

$$\bar{q}_y(z) = 1 + e^{\left(1 - \frac{z}{z_{jet}}\right)} \left[\frac{H_z}{H_\rho} \left(1 - \frac{z}{z_{jet}}\right) + \frac{2}{z_{jet}} - \frac{z}{z_{jet}^2} \right] \tag{134}$$

In Figure 11 we see that a westerly jet at the latitude of the AEJ only serves to enhance the β effect and hence $\bar{q}_y$ remains positive throughout the vertical, except at the ground where the boundary PV $\bar{q}_y < 0$ (due to $\theta_y < 0$). Since $u(z) > 0$ for $z > 0$ the Fjortoft criterion is also satisfied for a westerly jet. Thus baroclinic instability is possible via one CRW formed on the negative temperature gradient at the ground and another formed on the positive PV gradient somewhere in the jet.

Recalling (43), the evolution of amplitude is proportional to $\bar{q}_y$. Therefore, since

$|\bar{q}_y|$ is greater for the westerly jet, baroclinic growth will faster than for the easterly jet (this is examined in the following section). This illustrates the asymmetry between easterly and westerly jets due to the β effect stated in Section 1.2.
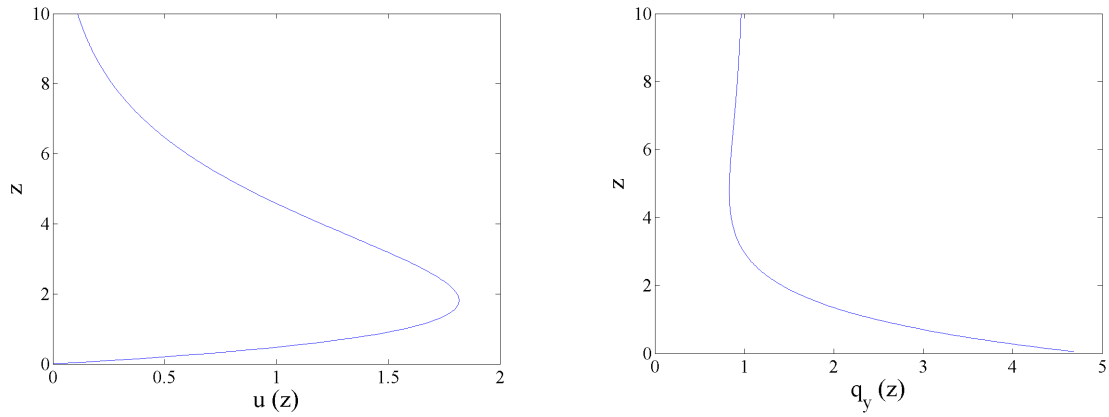

Figure 11: Basic state zonal velocity (left) and PV gradient (right) against height for a westerly jet. All variables non-dimensional.

5 Dispersion relation and structure

With a pair of CRW's shown to be possible, we now turn our attention to the normal mode problem and to the rate of growth to which they can lead. We recall:

$$\frac{\partial \tilde{q}}{\partial t} = -ik \left[\bar{u} \int_0^\infty \delta(z-h)\tilde{q}(h)dh + \frac{\partial q}{\partial y} \int_0^\infty G(z,h)\tilde{q}(h)dh \right] \qquad (135)$$

Alternatively:

$$\dot{\mathbf{q}} = \mathbf{A}\mathbf{q} \qquad (136)$$

where $\mathbf{q}$ is the vector containing $\tilde{q}_i = \tilde{q}(z_i)$ values for $i=0,1,...,N$ and $\mathbf{A}$, the linear dynamical operator, is the matrix of coefficients describing the effect of $\tilde{q}_i$ on the evolution of $\tilde{q}_j$ for $i,j=0,1,...,N$. The complex eigenvalues $\lambda_0, \lambda_1,..., \lambda_N$ satisfying:

$$\mathbf{A}\mathbf{q} = \lambda \mathbf{q} \qquad (137)$$

give the complex normal mode phase speeds c where:

$$q = q_0 e^{ik(x-ct)} = q_0 e^{ik(x-\text{Re}(c)t)} e^{k\text{Im}(c)t} \qquad (138)$$

Thus the GNM and DNM growth rates are given by:

$$\sigma_{\text{GNM}} = k \max \{\text{Im}(\lambda)\} \qquad \sigma_{\text{DNM}} = k \min \{\text{Im}(\lambda)\} \qquad (139)$$

i.e. the greatest and smallest (most negative) imaginary parts of eigenvalues multiplied by k. And the GNM phase speeds are given by the corresponding real parts of the eigenvalues. We note that the general solution to (136) is given by:

$$\mathbf{q}(t) = \mathbf{q}(0)e^{\mathbf{A}t} \qquad (140)$$

which illustrates that perturbations grow exponentially in the GNM.

5.1 Dispersion relation

We use the semi-analytic model with the linear dynamical operator obtained using the analytic Green functions to perform the above eigenanalysis for a range of wavenumbers. The growth rates obtained are shown in Figure 12 along with those for the equivalent westerly jet (see Section 4.2) and for the Charney model (uniform westerly shear) with the same parameters. For the easterly jet normal mode growth

38

occurs approximately in the region $0 < r < 0.5$ with waves longer than this ($r = 0.5$ corresponds to a dimensional wavelength of approximately 3000 km) unable to grow. The fastest growing wavelength is approximately $r = 0.22$ which is equivalent to a dimensional wavelength of 1500 km. We see that both the easterly jet and Charney model have greater growth rates and are able to sustain growth over a greater range of wavelengths. This reflects the restriction imposed by β on an easterly jet. We recall that growth rate is proportional to PV gradient (see (43)) which explains the high growth rate of the westerly jet (recalling the large PV gradient in Figure 11). In fact the westerly jet does not even seem to have a long wave cut-off as the other two plots do. We suspect that this is due to a superimposition of growing modes from approximately $r = 0.55$ onwards; however, this is irrelevant to our interests in this study.

Also shown are the corresponding phase speeds, obtained as desribed above, up to the long-wave cut-off for the easterly jet. The phase speed is always negative for the easterly jet and always positive for the two, demonstrating that phase-locked CRW's always propagate with the shear. We see that, for an easterly jet, GNM phase speed increases with wavelength, approaching the speed of the jet core $z = -1.8$ as growth rate tends to zero, i.e. neutral waves are merely passively advected by the jet. For the fastest wavelength $r \approx 0.22$, the GNM phase speed is approximately equal to -0.9, i.e. half the speed of the jet core.
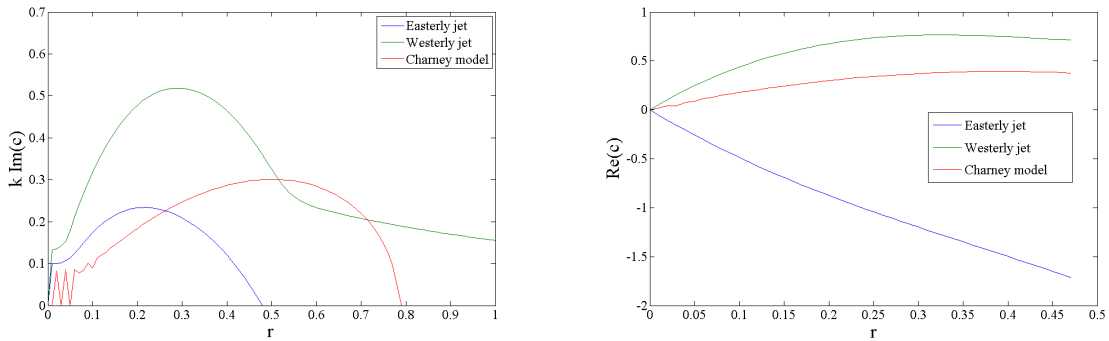

Figure 12: Left: Dispersion relation for growth rate against wavelength for easterly jet, westerly jet and uniform westerly shear, all with identical parameters. Right: dispersion relation for phase speed against wavelength for the same profiles. Density decays exponentially in all cases (see (16)). All variables non-dimensional.

5.2 Growing normal mode structures of PV and meridional wind

The full PV and meridional wind structures for the easterly jet are shown in Figure 13 for the fastest wavelength $r = 0.22$ and a near neutral wavelength $r = 0.45$ (see Figure 12). Note the resemblance, especially for $r = 0.22$, to Figure 5, i.e. positive and negative anomalies at the top of the perturbation are to the left of those at the bottom, allowing anomalies to be amplified as described in Section 2.1. The meridional wind is greatest at the ground where the boundary temperature wave dominates. For the longer, almost neutral wavelength, the perturbation extends further up, approaching $z \approx 1.5$ where the PV gradient ceases to be negative (see Figure 10). The growth rate of a PV structure extending to a height where the PV gradient is very small is since growth rate is proportional to PV gradient (see (43)). Since the Fjortoft condition (34) cannot be satisfied above this level and hence CRW's cannot phase-lock, as argued in Section 2.1, this is the height to which the top of the GNM PV structure tends as the growth rate tends to zero.

5.3 CRW structures

The observations in the previous subsection are reflected in Figure 14 where the vertical PV structures of the CRW's are given for the same two wavelengths as well as for the observed fastest growing wavelength for a westerly jet $r = 0.29$ (see Figure 12). A near neutral wavelength is not studied for a westerly jet because, as shown in Figure 12, this would be for $r >> 1$, where $r = 1$ is equivalent to approximately 7000 km (note the difference in scale for r to that used in the literature for mid-latitude parameters - see Section 2.6) and hence beyond the range of realistic wavelengths. In all cases, the upper CRW has a positive PV maximum (since the Green functions used are negative), which is sharp due to the change in sign of q_y above it which acts as a lid. The lower CRW's are less distinctive and, similarly to those for the Charney model in Figure 8, consisting of negative PV near the ground where the boundary PT gradient dominates. As the growth rate tends to zero (compare the first and second rows), the non-zero PV of both CRW's approaches the height of zero PV gradient $z \approx 1.5$, similarly to the top of the structure approaching this height in Figure 13 as explained. The CRW's for the westerly jet do not have the sharpness of those of the easterly jet since the PV gradient is positive throughout the interior. Note the likeness of the CRW's for the westerly jet (especially the upper CRW) to those shown for the Charney model in Figure 8. It seems that, for westerly shear
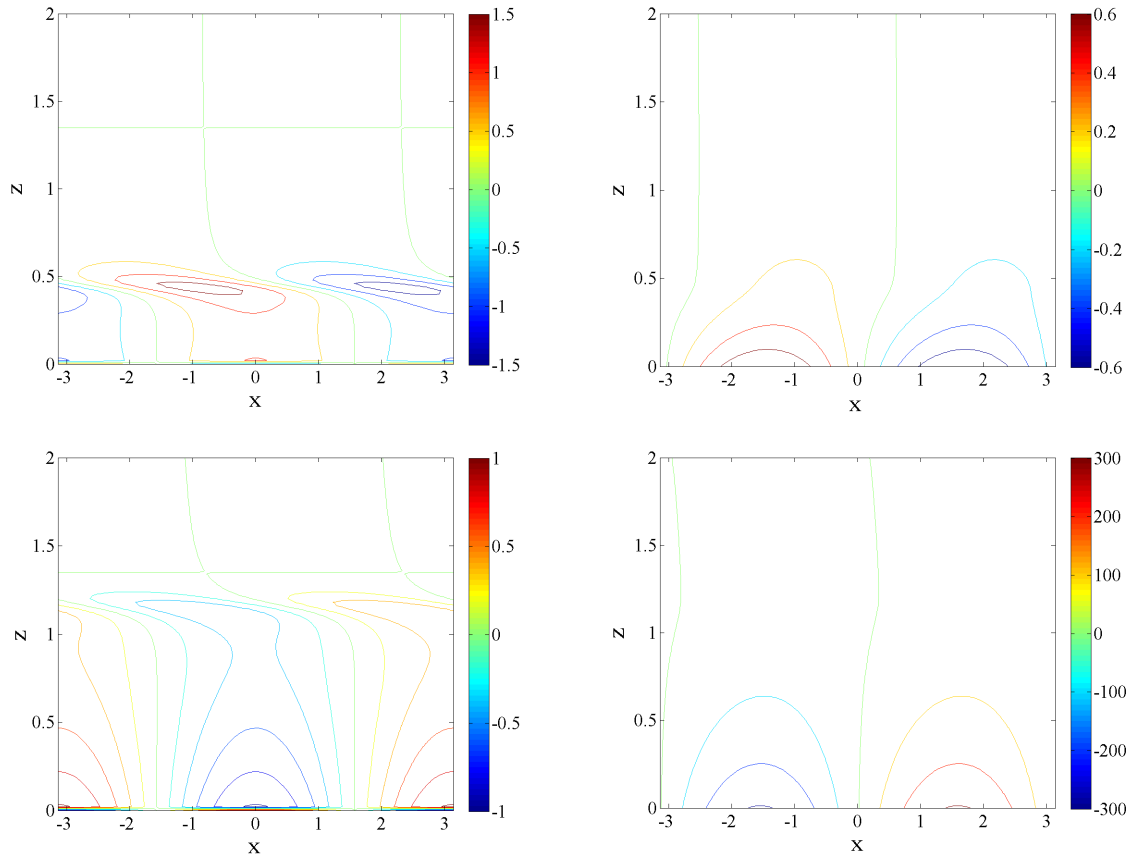
Figure 13: GNM PV (left) and meridional wind (right) on the x-z-plane for $r = 0.22$ (top) and $r = 0.45$ (bottom). Note the changes of scales between all plots. All variables non-dimensional.

(where β does not need to be cancelled), the presence of a jet as opposed to linear shear, does not significantly change the structures by which baroclinic instability is possible (although, from Figure 12, the growth rate is significantly increased).

6 Initial Value Problem

We are now interested to see how a given initial PV structure will evolve within time t_{AEJ} on the AEJ. We have seen the normal mode growth that the AEJ allows. However, this does not describe the full evolution of the perturbation as there are other mechanisms at work before the CRW's phase-lock. General initial conditions may include PV that did not arise from displacements of the zonally symmetric state. Therefore, following De Vries *et al.* (2009), the perturbation PV is partitioned as $q = q_d + q_p$ where q_p is known as the *passively advected residual PV* (PAR PV). The PAR PV is merely advected by the shear flow and is neutral (can not amplify). However, as described in Section 6.1, it can still lead to growth.

6.1 Various growth mechanisms

Following De Vries *et al.* (2009), the growth is partitioned into the following mechanisms:

- *Shear instability*, i.e. mutual growth via the interaction of two CRW's as described in Section 2.1.

- *Resonance*. This refers to excitation of the CRW's by meridional advection associated with interior PAR PV in the same way as the CRW's excite one another. However, since the PAR PV is neutral, the CRW's cannot amplify the PAR PV in return and so this is a one-way mechanism and hence linear.

- *The Orr mechanism*. This describes the effect that the shear has on the interior PAR PV, known since the work of Orr (1907). If we consider a breakdown of the PAR PV into that at each level in the interior, the PAR PV elements (called *PV building blocks* by de Vries(2006)) at each level are passively advected and so do not interact with one another. If we have an initial PV structure consisting of structurally similar but out-of-phase PV building blocks then over time the shear disperses the initial PV structure. Thus the streamfunction amplifies for an initial upshear tilt and decays for an initial downshear tilt, altering the kinetic energy of the perturbation. The crucial distinction of this mechanism is that, although the streamfunction is amplified, the PV is not, which makes it easy to spot that the Orr mechanism, as opposed to the other two considered, is responsible for observed energy growth.

Together, the resonance and Orr mechanisms are the linear transient effects referred to in Section 1.2. We seek to establish the extent to which these, as opposed to CRW

interaction, are responsible for growth of AEW's for a range of initial conditions.

6.2 Simple initial conditions

The simplest initial conditions are a PV monopole (alternating positive and negative anomalies) and a dipole (two layers of alternating positive and negative anomalies, half a wavelength out of phase). These are shown in Figure 15 along with the corresponding meridional wind obtained using the Green function method. Such structures are used by De Vries *et al.* (2009) for the Charney model. The validity of using them as initial disturbances is beyond the scope of this project. For now we use them merely to illustrate how simple wave-like structures will develop on the AEJ.

6.3 Tilting of structures

As discussed in Section 2, the phase difference at time t between the upper and lower PV anomalies determines their mutual amplification and phase adjustment at t. Since the Charney Stern and Fjortoft conditions are satisfied (equations (33) and (34)), phase-locking will eventually occur for any initial PV perturbation and the growing normal mode will be reached. However, due to the finite time available for waves to propagate along the AEJ, there is limited time available for this to happen and so growth may be minimal. Therefore we seek to establish the growth that will occur for a given phase difference between the top and bottom of an initial PV monopole or dipole.

We define the tilt of a perturbation as the phase difference between the PV anomalies at the top and bottom of the perturbation divided by the vertical distance between them (the *depth* of the perturbation), normalised by wavelength $r = \frac{1}{2k}$. For a perturbation with constant tilt throughout the vertical, this is equivalent to the phase difference between the anomalies at z and the ground divided by z for any z. Since the length and height scales are related by $L = \frac{N}{f_0} H_z$, this is therefore given by $M \frac{L}{H} \frac{k}{r} = \frac{N}{2f_0} M$ where M is parameter such that $M = 0$ implies zero tilt and $M = \pm \frac{1}{2}$ and $-\frac{1}{2} < M < \frac{1}{2}$ gives the full range of possible tilt.

We wish to know the effect of the tilt in the initial PV structure on growth during the time available for waves to propagate along the AEJ. We measure growth by the log of the ratio of total energy $\text{TE}(t)$ of the perturbation at time t_{AEJ} to total

energy at $t = 0$ where:

$$E(t) = \log\left(\frac{TE(t)}{TE(0)}\right) \tag{141}$$

where total energy is the sum of kinetic energy and available potential energy and is given by (Pedlosky (1990)):

$$TE = -\frac{1}{2}\left(\{\psi, q\} + \{q, \psi\}\right) \tag{142}$$

where $\{p, q\} = \frac{1}{2}\int\int p * q\bar{\rho}\, dydz$ and $p*$ denotes the complex conjugate of p. Since M is a measure of phase difference, normalised by wavelength, a plot of M against E will have a period in the M-axis of 1. We compare the wavelength with the fastest GNM $r = 0.22$ (from Figure 12) and an almost neutral wavelength $r = 0.45$ for an initial monopole and an initial dipole. Figure 16 shows the relationship between tilt and energy growth, where in each case M is plotted between $\frac{1}{2}$ and $-\frac{1}{2}$. We notice that in all the plots in Figure 16, $E > 0$ for $M < 0$, i.e. the total energy of the perturbation always increases when the initial PV structure is tilted upshear. Note that for a positive tilt (as is the case in the GNM for an easterly (negative) shear - see Figure 3) growth via CRW interaction is much greater. Therefore, since the total energy growth in this time is much greater for negative tilt than positive tilt, this suggests that the Orr mechanism is playing a much greater role than CRW interaction (even in the case of the wavelength with the fastest growing normal mode). This will be quantified in Section 7.

6.4 Time evolution for optimally tilted initial PV structures

Using the optimal tilt obtained in each of the plots in Figure 16, we now use the KRW amplitude and phase evolution equations (122) and (123) to model the evolution of PV during the time taken to cross the AEJ in each case. Recalling (12), this time is found to be $t = 5.03$ which is approximately equal to 5 days.

6.4.1 Monopole

In Figures 17 and 18, the evolution of PV and induced meridional wind is shown at $t = 0$, $t = 2.5$ and $t = 5$ for an initial monopole for the two wavelengths we are examining. In both cases we notice the PV structure untilting over time due to the shear, suggesting the Orr mechanism being highly active during this time. The shape of the initial structure is altered more for shorter waves due to the greater ratio between shear and wavelength. We notice that, for both wavelengths, at $t = 2.5$,

although there is significant increase in the meridional wind, the PV amplitude is no greater. This strongly suggests that the Orr mechanism is dominant during this time. For the shorter (faster growing) wavelength, the maximum PV amplitude more than doubles between $2.5 < t < 5$, meaning that CRW interaction may take place during this time. However, the PV at $t = 5$ does not particularly resemble the GNM for the same wavelength so we suspect that this growth is largely due to resonance. For the longer (almost neutral) wavelength, there is only slight increase in amplitude at $t = 5$, suggesting that growth by CRW interaction is very small.

6.4.2 Dipole

In the case of the dipole (Figures 19 and 20), due to the extra complexity of the structure and same-signed anomlies not being aligned, it is more difficult for the shear to untilt the structure. The two layers become increasingly disparate, making it increasingly difficult for interaction to occur throughout the perturbation. In the case of the longer wavelength, there is little difference in either structure or magnitude, suggesting none of the mechanisms are particularly active.

7 Optimal growth

7.1 Singular vector analysis

Having observed the evolution of simple PV structures, we now wish to discover the initial PV structure for which growth is greatest over the given time t_{AEJ}. We recall the linear dynamical operator $\mathbf{A}$, defined in (117), where $\dot{\mathbf{q}} = \mathbf{A}\mathbf{q}$ and $\mathbf{q} = \mathbf{Q}e^{i\epsilon}$ for amplitude and phase vectors $\mathbf{Q},\epsilon$. There must be some $\mathbf{q}_0$ such that, for the optimisation time t_{opt}, $\mathbf{q}(t_{opt})$ is maximised for a given norm. As we are interested in energy growth, this is the norm for which we shall calculate this optimum initial condition and our optimisation time is t_{AEJ}. The optimal perturbation can be obtained by **singular value** (SV) analysis (Farrell (1982)) of $\mathbf{A}$ where, since $\mathbf{A}$ is an N×N matrix (where N is the number of levels at which z is defined in the discretisation), N SV's are obtained. The one giving the greatest energy growth, the leading SV, is then the initial $\mathbf{q}$ vector that maximises total energy growth within time t_{AEJ}.

The singular vector analysis is complex and need not be given here. However, the relevant code to obtain the leading SV is included in the semi-analytic model written by Hylke de Vries. The SV structures obtained for $r = 0.22$ and $r = 0.45$ are shown in the top left panels of Figures 21 and 22 respectively and their full evolution at $t = 0$, $t = 2.5$ and $t = 5$, along with the induced meridional wind, follows in the same figures. We notice that the SV looks remarkably similar to the optimally tilted monopole (see the top left panels of Figures 17 and 18) for both wavelengths. The main differences are that the SV is slightly curved to compensate for the curvature of the jet and does not extend as high as the chosen monopoles (whose maximum heights were chosen arbitrarily). For $r = 0.22$ (the wavelength with the fastest GNM growth) the maximum height is at approximately $z = 0.6$, one third of the height of the jet core, so that, for an optimal perturbation, the interaction takes place in the region where the PV gradient is greatest (most negative - see Figure 10). For the longer wavelength $r = 0.45$ the SV extends higher but it is still within the region where the PV gradient is negative.

In the evolution of PV and meridional wind, we notice much greater amplitudes than the plots in Section 6. As for the initial monopole, for both wavelengths there is minimal growth in PV amplitude for $0 < t < 2.5$ meaning that the Orr mechanism is responsible for most of the growth in this time (which must be significant since this is the leading singular vector). As for the monopole, during $2.5 < t < 5$, the

maximum PV amplitude doubles for both wavelengths, thus the resonance and/or CRW interaction mechanisms are active during this time. For the near neutral wavelength $r = 0.45$, the final PV structure does not much resemble that of the GNM for the same wavelength (see Figure 13). Therefore we suspect that the observed doubling of PV amplitude is mainly due to resonance. For $r = 0.22$ however, at final time, both the PV and meridional wind strongly resemble those of the GNM for the same wavelength, suggesting that the CRW's have phase-locked at t_{AEJ} and hence CRW interaction may have been a significant part of the observed growth in amplitude.

The observations we have made from these figures are highly useful for diagnosing aspects of the growth of these optimal perturbations as described. However, there still exists a large uncertainty as to whether resonance or CRW interaction are responsible for the growth in PV anomaly amplitude at later times. Also, since the Orr mechanism does not amplify the anomalies, we cannot compare its growth to that of CRW interaction. We therefore seek a means of quantifying the growth from CRW interaction as a fraction of the total perturbation growth.

7.2 Total energy growth for the leading singular vector

We are interested in how much of the total perturbation energy at $t = t_{\mathrm{AEJ}}$ is due to the CRW's. In order to discover this, we note that, in the GNM, the total energy $\mathrm{TE_{GNM}}(t)$ evolves with exponential growth rate σ_{TE}:

$$\mathrm{TE_{GNM}}(t) = \mathrm{TE}_0 e^{\sigma_{\mathrm{TE}} t} \tag{143}$$

where $\sigma_{\mathrm{TE}} = 2\sigma_{\mathrm{GNM}}$ (because TE is of order of magnitude of the perturbation squared), which is equal to 0.47 for $r = 0.22$ and 0.13 for $r = 0.45$. Figure 23 shows $\log\left(\frac{\mathrm{TE_{GNM}}(t)}{\mathrm{TE}(0)}\right) = \sigma_{\mathrm{TE}} t$ plotted against time for $0 \leq t \leq 20$ in the cases of each of the wavelengths $r = 0.22$ and $r = 0.45$. Also plotted is $E(t) = \log\left(\frac{\mathrm{TE}(t)}{\mathrm{TE}(0)}\right)$, using the singular vector as the initial perturbation PV. For both wavelengths, $E(t)$ eventually becomes a straight line with the same gradient σ_{TE} as the GNM plot, indicating exponential growth due to CRW interaction alone from this point on. For $r = 0.22$, this occurs at approximately $t = 5 \approx t_{\mathrm{AEJ}}$, confirming that the CRW's have phase-locked (as we previously suspected from comparing the PV structure in Figure 21 at $t = 5$ with that of the GNM for the same wavelength). For $r = 0.45$, the total energy in fact decreases after $t = t_{\mathrm{AEJ}}$, suggesting that decay associated

with the transient mechanisms dominates before the CRW's eventually phase-lock at approximately $t = 10$. This confirms that the growth in amplitude for this near neutral wavelength for $2.5 < t < 5$ observed in Figure 22 is mainly due to resonance.

We can now compare total energy growth with that which would be attained by a GNM (CRW's in a phase-locked configuration). At $t = t_{\mathrm{AEJ}}$, the ratio is:

$$\frac{\mathrm{TE}_{\mathrm{GNM}}(t_{\mathrm{AEJ}})}{\mathrm{TE}(t_{\mathrm{AEJ}})} \tag{144}$$

which is equal to 0.029 for $r = 0.22$ and 0.023 for $r = 0.45$. So, for both a fast-growing and an almost neutral wavelength, with the leading singular vector for $t_{\mathrm{opt}} = t_{\mathrm{AEJ}}$ as the initial perturbation, energy growth during the time taken to cross the AEJ is almost entirely due to transient effects.

8 Conclusions and further work

8.1 Conclusions

We have seen that a vertical profile of zonal wind with the observed characteristics of the African easterly jet has sufficient curvature to cancel the planetary vorticity gradient β at a range of altitudes between the ground and somewhere below the jet core. This means that a negative interior PV gradient exists at these altitudes. Boundary temperature anomalies formed on the positive temperature gradient at the ground act as PV anomalies and form a westward (relative to the basic state zonal flow) propagating wave which can create anomalies in the interior and form an eastward propagating wave there due to the negative PV gradient. This means the Charney-Stern criterion is satisfied and so a pair of CRW's can indeed be formed on the AEJ. Since the basic state zonal flow at the positive temperature gradient at the ground is greater (less negative) than at the negative PV gradient in the interior, the Fjortoft criterion is also satisfied and growth via baroclinic instability is therefore possible.

Addressing the questions posed in Section 1.2:

1. For a basic state defined by AEJ characteristics, the wavelength for an AEW that supports the fastest growth via CRW interaction is 1515 km. At this wavelength the GNM growth rate is by a factor of 0.23 per day and the GNM phase speed is 6ms^{-1} westwards (relative to the ground) which is half the jet maximum velocity. For wavelengths longer than approximately 3500 km, normal mode growth is infinitesimal and hence, unless an unrealistic amount of time is available, it cannot make any significant contribution to the development of the perturbation.

2. The finite time available for CRW's to develop into the GNM means that the initial perturbation is crucial and, unless it is suitably tilted, there is insufficient time for the wind shear to take the PV structure into the GNM. However, for initial PV structures tilted in a mutually amplifying configuration, the total growth is minimal or even negative. For an initial upshear tilt, the shear always acts to reverse the tilt of the PV and the energy of the perturbation is always greater at time t_A than to begin with, even though the PV amplitudes remain fairly similar. Therefore the Orr mechanism is highly active for AEW's and counter-acts CRW interaction within the given time. Growth is

significantly greater for an initial monopole than for a dipole.

Although providing very low normal mode growth rates, waves as long as 3000 km (as compared to the fastest growing wavelength for normal modes in Sections 6 and 7) still lead to reasonably similar total energy growth within the time of propagation across the AEJ. Longer waves require less initial tilt (as a fraction of wavelength) for total growth to be maximised. The leading singular vector representing the optimal perturbation for time t_{AEJ} is remarkably similar to the monopole with optimal initial tilt. This suggests that the AEJ favours simple initial perturbations.

3. At both wavelengths studied, the PV amplitude of the singular vector hardly changes in the first half of the time to cross West Africa ($0 < t < 2.5$), indicating that the energy growth is dominated by the Orr mechanism. In the second half ($2.5 < t < 5$), the PV amplitude approximately doubles and (at the smaller wavelength) the growth rate gradually reduces to that of the GNM, indicating that the resonance mechanism is dominant in this time before CRW interaction takes over. Thus CRW's on the AEJ can indeed phase-lock within the time taken to cross west Africa at the speed of the jet maximum. Longer waves do not phase-lock in the allowed time and for $r = 0.45$ this appears to happen after $2t_{\mathrm{AEJ}}$. At this wavelength the resonance mechanism dominates and there is in fact decay of total energy before the CRW's phase-lock.

Even for the short wavelength where phase-locking occurs, the GNM growth rate is not sufficiently large for growth via CRW interaction to be significant during the limited time window when compared to the linear transient growth mechanisms which inevitably dominate at short times. For the wavelength giving the fastest GNM, the normal mode energy at t_A is only 3 per cent of the total perturbation energy and the mean log growthrate of the GNM during this time is less than half that of the total perturbation. And for longer waves these ratios are even smaller.

8.2 Further work

In this study two major assumptions have been made, the validity of each of which should be investigated.

- Firstly a purely baroclinic flow has been studied so that the zonal flow is independent of y. Due to the approximate thermal wind balance, the vertical shear is inevitably more significant but a 3-D jet should be considered to estalish the extent to which meridional variations in zonal velocity play a role.

- In the PV equation $Dq = 0$, it is assumed that there are no frictional or diabatic effects and it is this equation which has formed the foundation of all the work here. de Vries, Methven and Frame (2010) develop a theoretical framework for the evolution of extratropical baroclinic waves with a parameterisation of latent heat release based on the notion that hot air rises and cool air descends. In this model, assuming a negative temperature gradient, warm moist air from the south ascends and becomes saturated while cool dry air from the north descends. However, in west Africa, the correlation between moisture and temperature is reversed due to the Sahara desert, meaning that warm dry air from the north ascends and cool moist air from the south descends. Hence saturation does not occur since it is dry air that rises. Therefore a new parameterisation of latent heat release in baroclinic waves is required to allow for this unusual situation.

References

Bretherton, F. (1966). Critical layer instability in baroclinic flows. *Q. J. R. Meteorol. Soc.*, **92**, 325–334.

Charney, J. (1947). The dynamics of long waves in a baroclinic westerly current. *J.Meteorol.*, **4**, 135–163.

Charney, J. and Stern, M. (1962). On the stability of internal baroclinic jets in a rotating atmosphere. *J. Atmos. Sci.*, **19**, 159–172.

De Vries, H., Methven, J., Frame, T., and Hoskins, B. (2009). An interpretation of baroclinic initial value problems: Results for simple basic states with nonzero interior PV gradients. *J. Atmos. Sci.*, **66**, 864–882.

Fjørtoft, R. (1950). Application of integral theorems in deriving criteria of stability for laminar flows and for the baroclinic circular vortex. *Geofys. Publ.*, **17**, No. 6, 1–52.

Heifetz, E. and Methven, J. (2005). Relating optimal growth to counter-propagating Rossby waves in shear instability. *Phys. Fluids*, **17**, 064107.

Heifetz, E., Bishop, C., Hoskins, B., and Methven, J. (2004a). The counter-propagating Rossby wave perspective on baroclinic instability. Part I: Mathematical basis. *Q. J. R. Meteorol. Soc.*, **130**, 211–231.

Heifetz, E., Methven, J., Hoskins, B., and Bishop, C. (2004b). The counter-propagating Rossby wave perspective on baroclinic instability. Part II: Application to the Charney model. *Q. J. R. Meteorol. Soc.*, **130**, 233–258.

Hoskins, B., McIntyre, M., and Robertson, A. (1985). On the use and significance of isentropic PV maps. *Q. J. R. Meteorol. Soc.*, **111**, 877–946.

Lindzen, R., Farrell, B., and Tung, K. (1980). The concept of wave over-reflection and its application to baroclinic instability. *J. Atmos. Sci.*, **37**, 44–63.

Methven, J. and de Vries, H. (2008). Comments on "Piecewise Potential Vorticity Inversion: Elementary tests. *J. Atmos. Sci.*, **65**, 3003–3008.

Orr, W. (1907). The stability or instability of the steady motions of a perfect fluid and of a viscous fluid. *Proc. Roy. Irish Acad.*, **A27**, 9–138.

Thorncroft, C., Hall, N., and Kiladis, G. (2008). Three-dimensional structure and dynamics of African Easterly Waves. Part III: Genesis. *J. Atmos. Sci.*, **65**, 3596–3607.
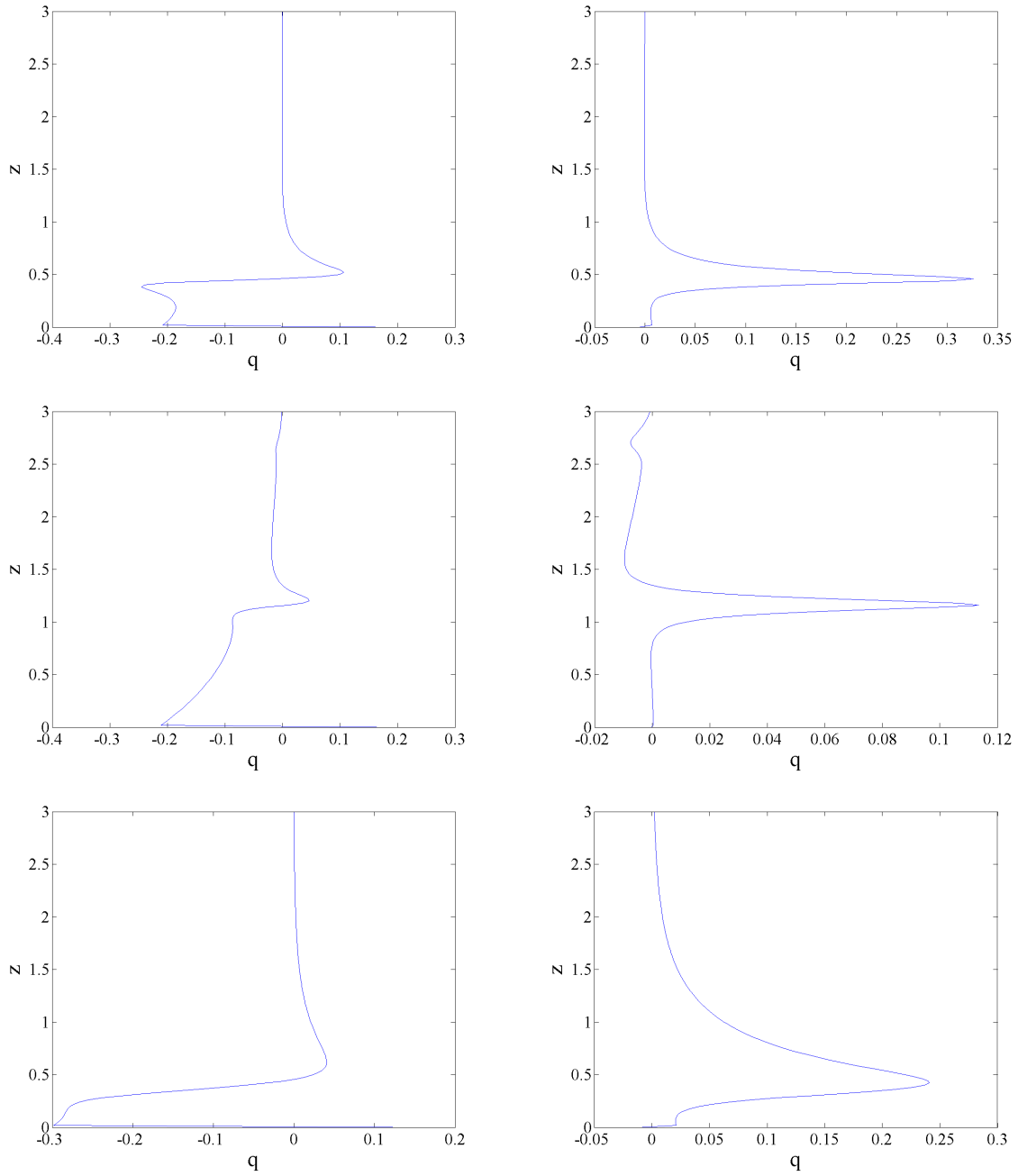
Figure 14: Vertical PV structure for lower CRW's (left) and upper CRW's (right). Top row is for an easterly jet with $r = 0.22$. Second row is for an easterly jet with $r = 0.45$. Bottom row is for a westerly jet with $r = 0.29$. All variables non-dimensional.
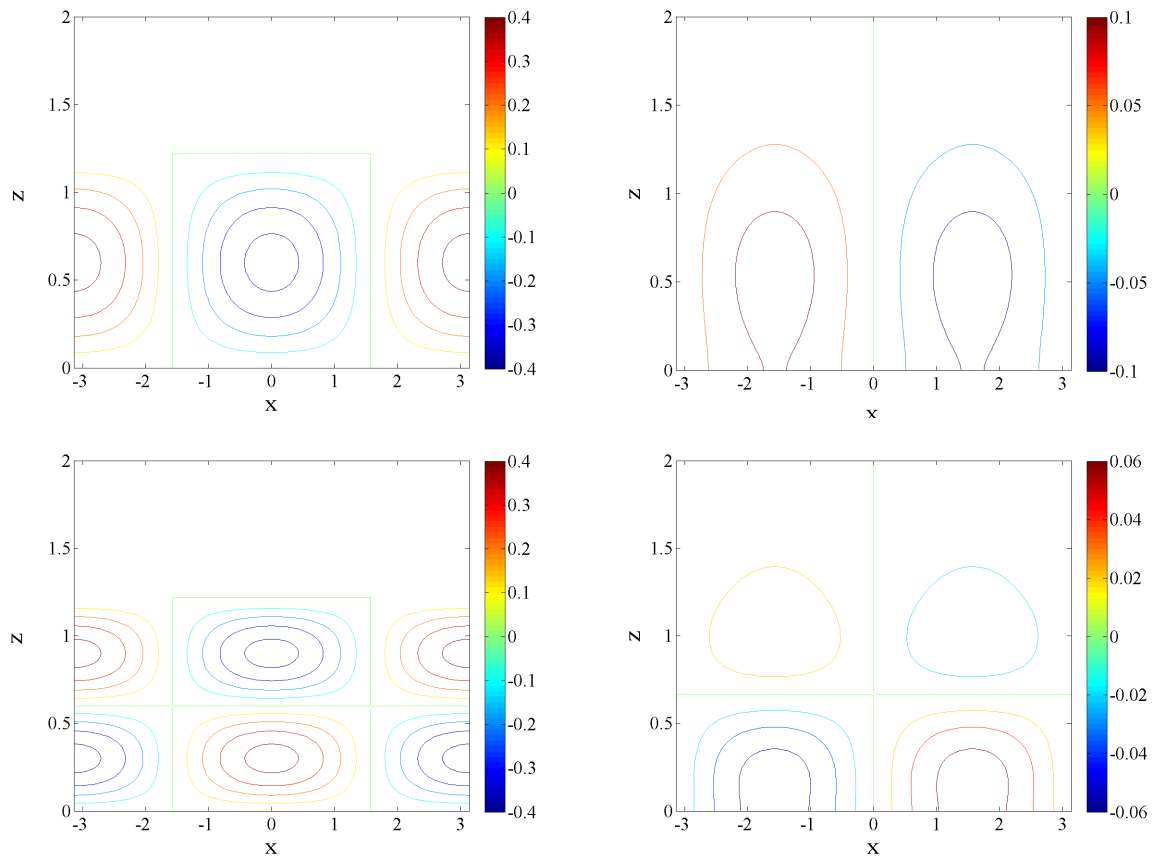
Figure 15: Initial PV (left) and induced meridional wind (right) on the x-z plane for an untilted monopole (top) and dipole (bottom). Note change of scale for meridional wind between top and bottom plots. All variables non-dimensional.
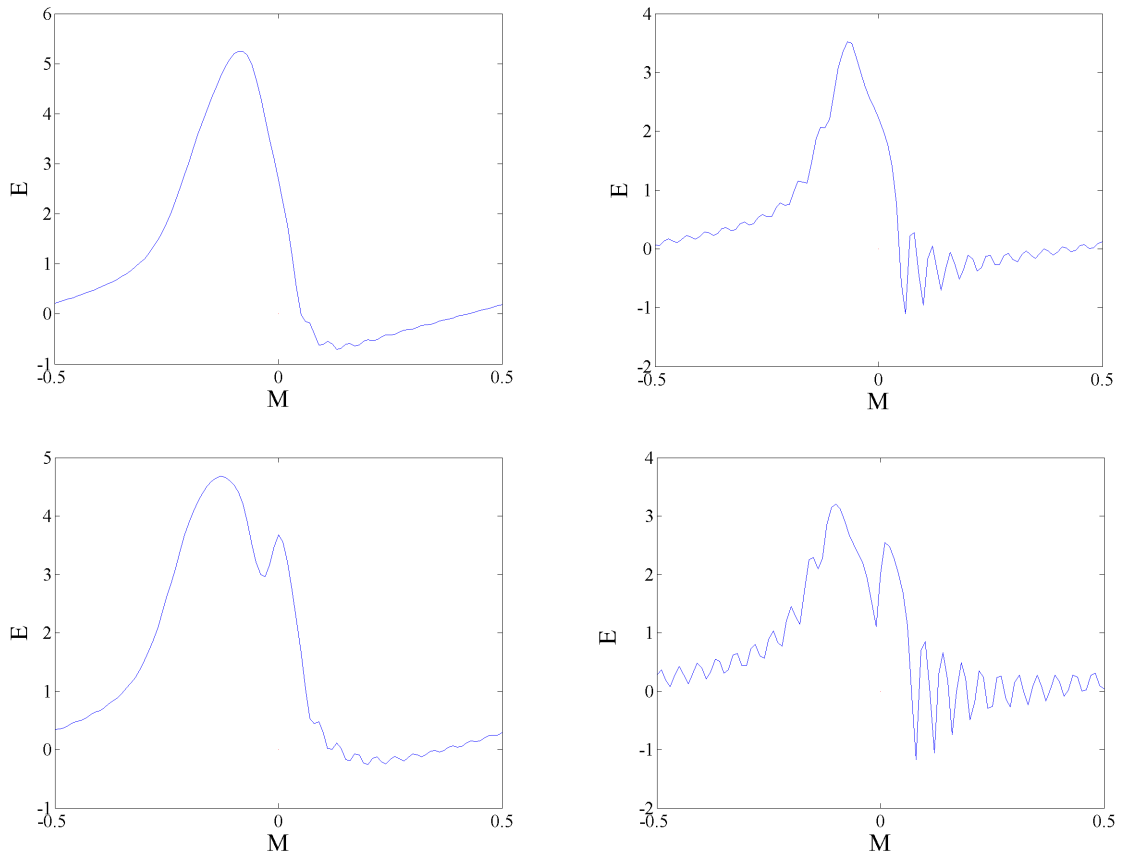
Figure 16: Tilt of initial PV monopole for $r = 0.22$ (top left), PV monopole for $r = 0.45$ (top right), PV dipole for $r = 0.22$ (bottom left) and PV dipole for $r = 0.45$ (bottom right) against log energy amplification at $t = t_{\mathrm{AEJ}}$. Note changes of scale between plots. All variables non-dimensional.
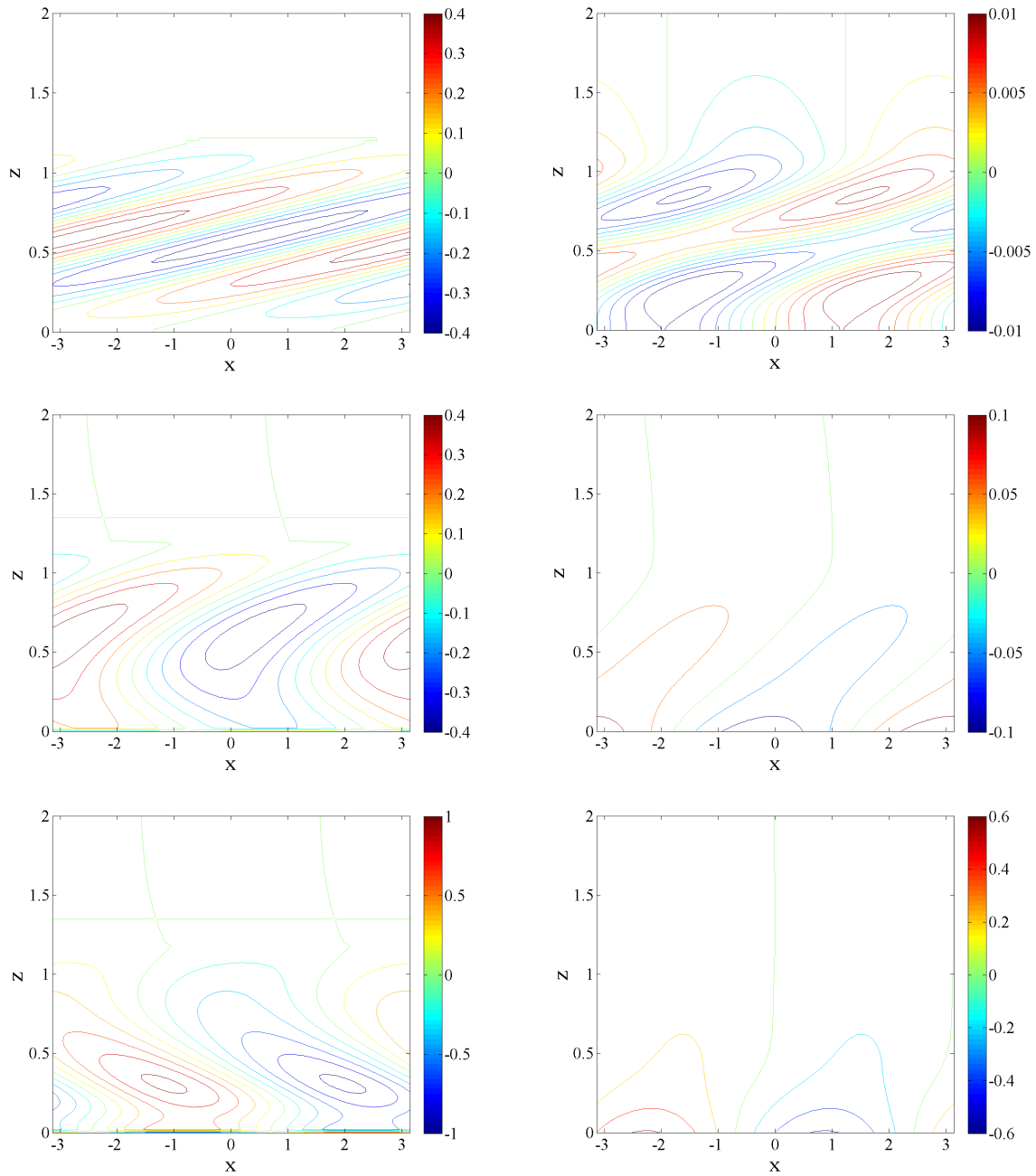
Figure 17: Evolution of PV (left) and meridional wind (right) on the x-z-plane for an initial monopole with optimal tilt for the wavelength of the fastest GNM $r = 0.22$ at $t = 0$ (top), $t = 2.5$ (middle) and $t = 5$ (bottom). Note the changes of amplitude between plots. All variables non-dimensional.
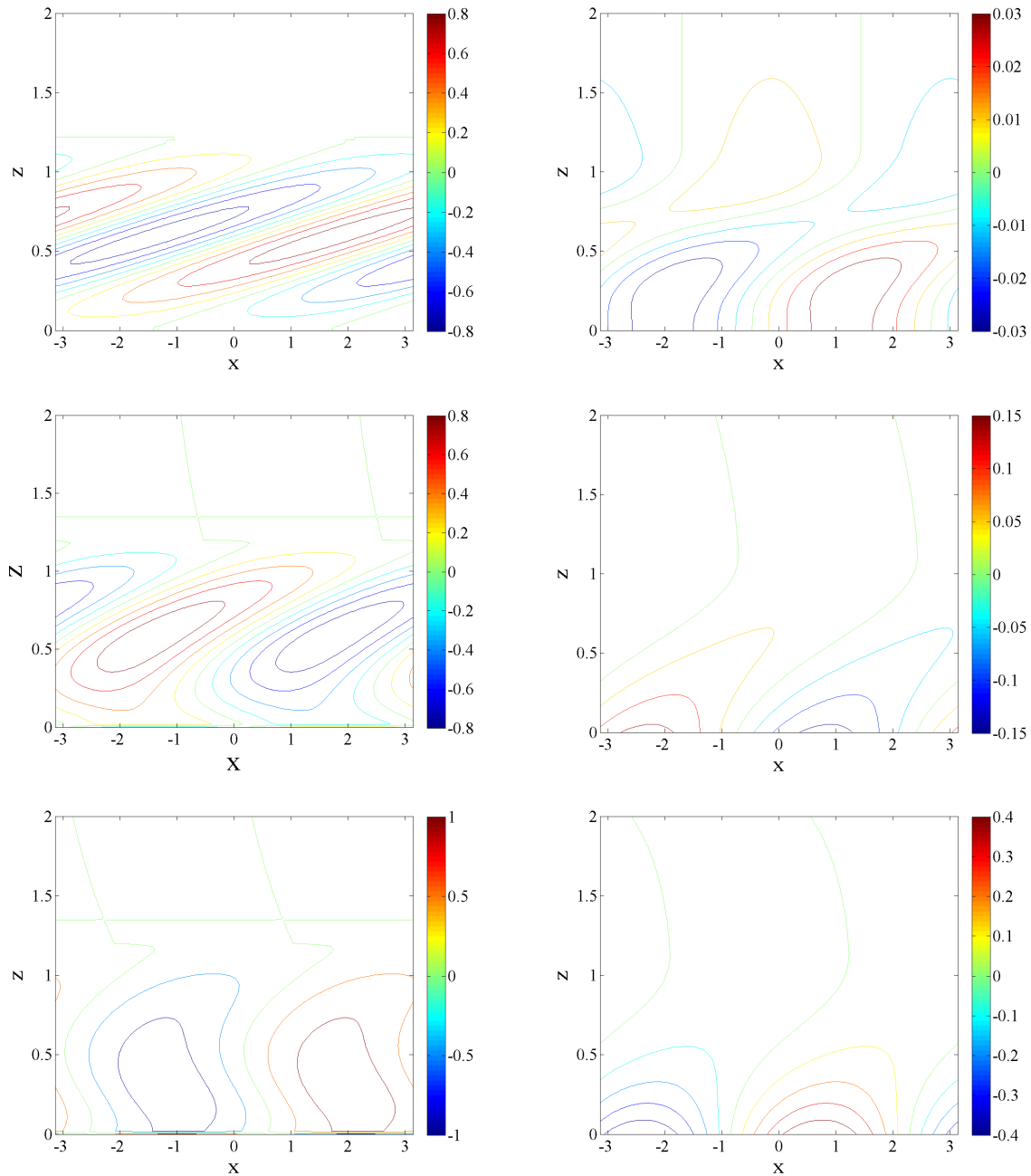
Figure 18: As for Figure 17 but for near neutral neutral wavelength $r = 0.45$.
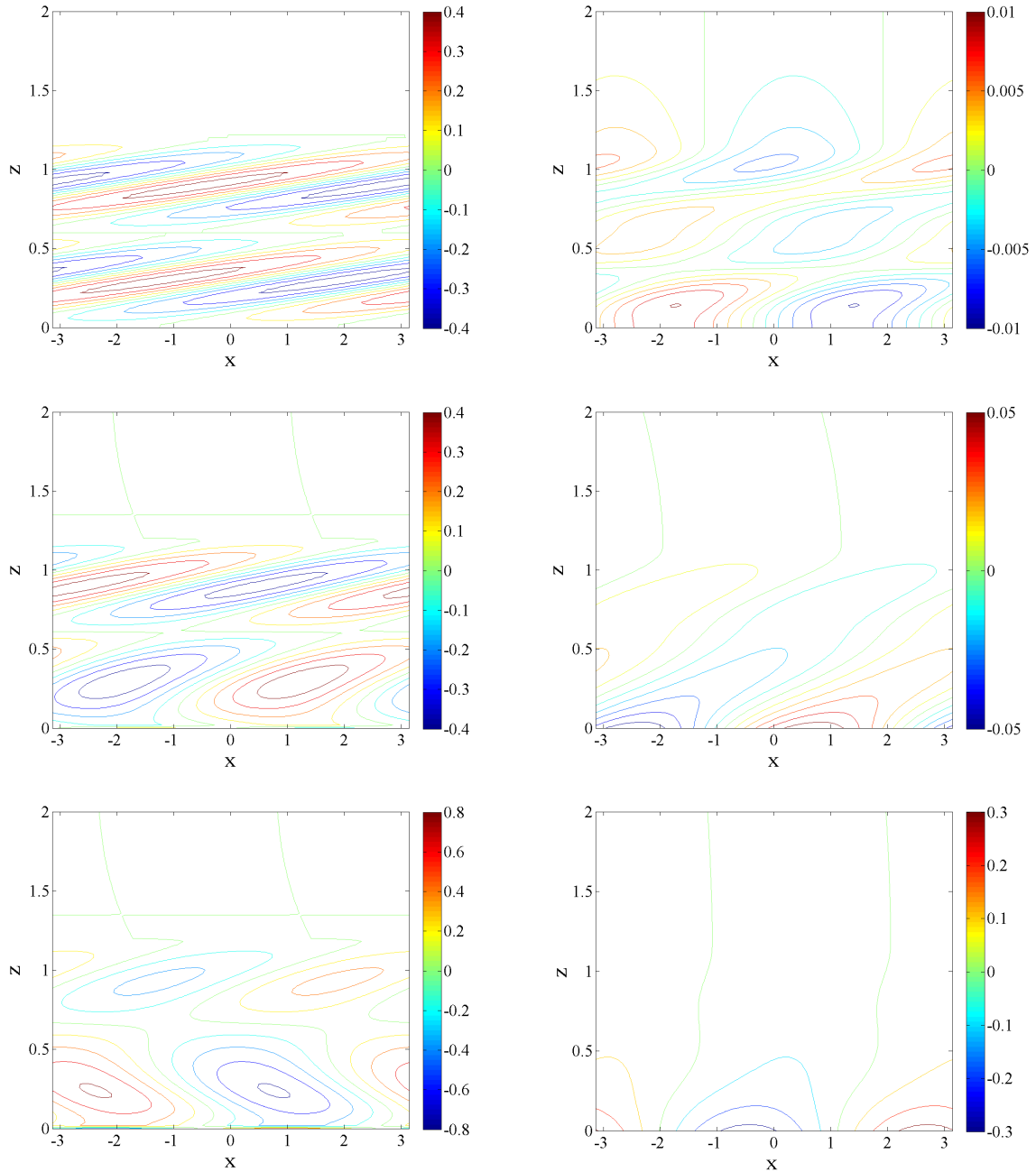
Figure 19: As for Figure 17 but for an initial dipole with optimal tilt.
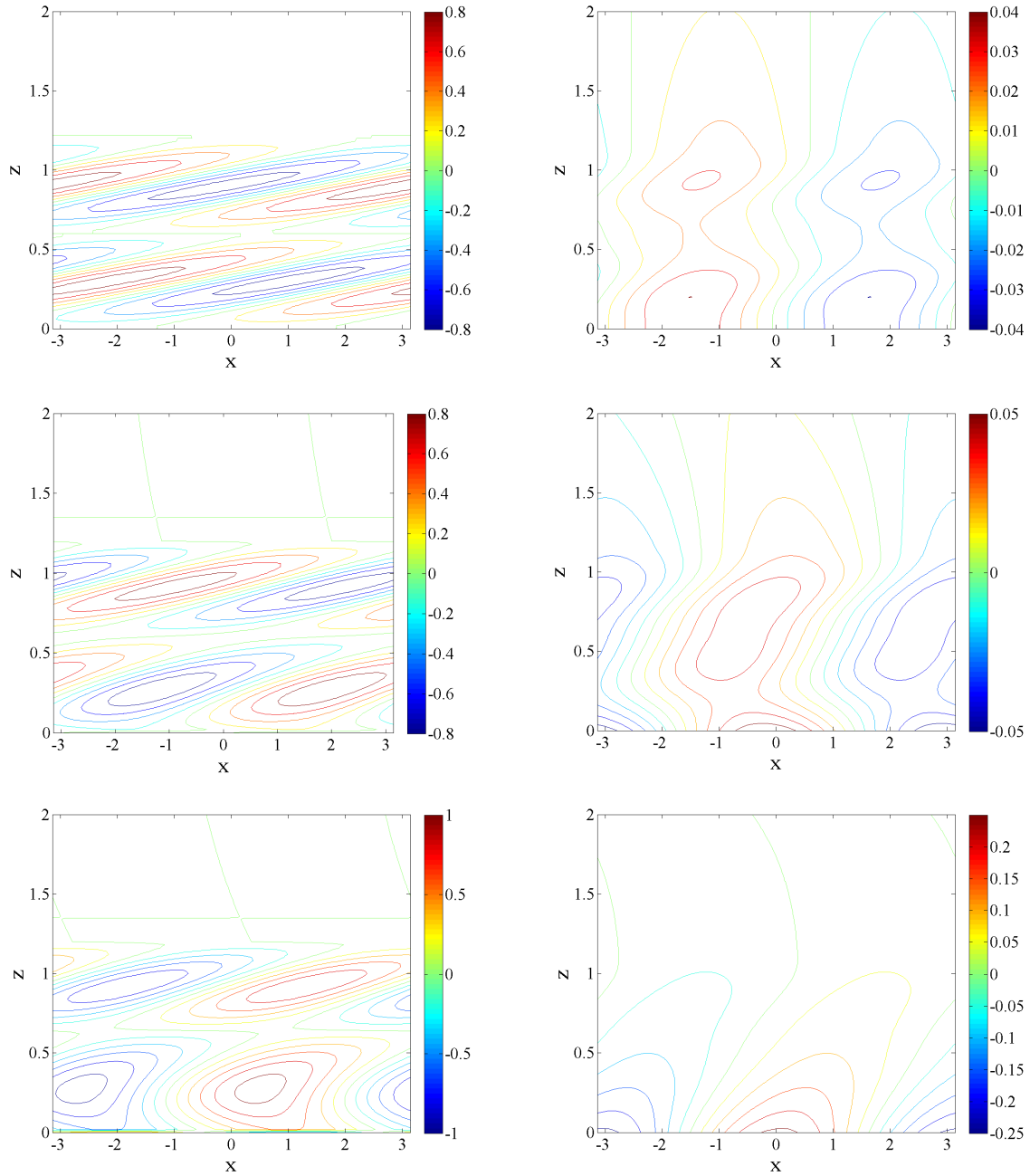
Figure 20: As for Figure 19 but for near neutral wavelength $r = 0.45$.
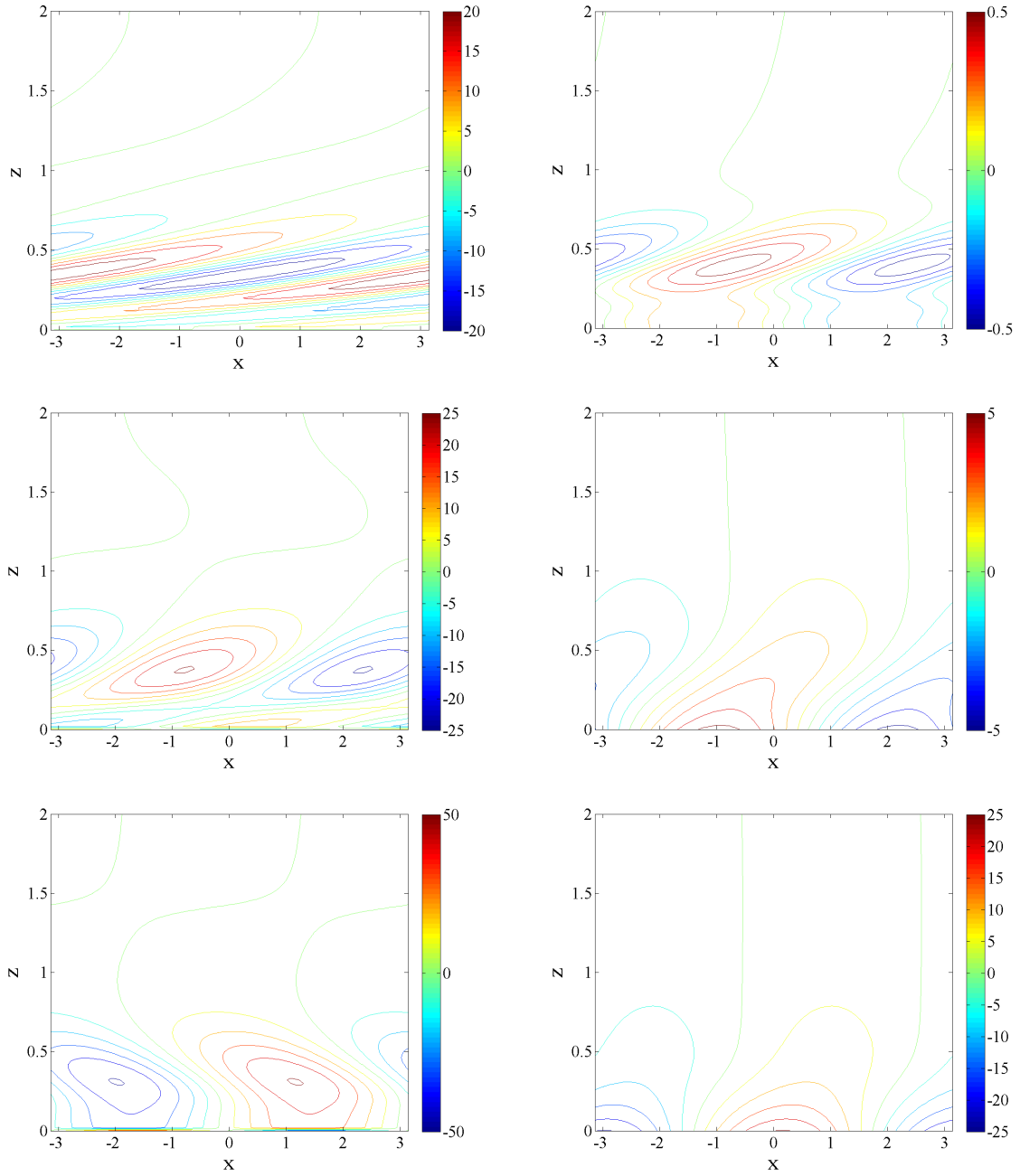
Figure 21: Evolution of PV (left) and meridional wind (right) on the x-z-plane for the leading singular vector for $r = 0.22$ at $t = 0$ (top), $t = 2.5$ (middle) and $t = 5$ (bottom). Note the changes of amplitude between plots. All variables non-dimensional.
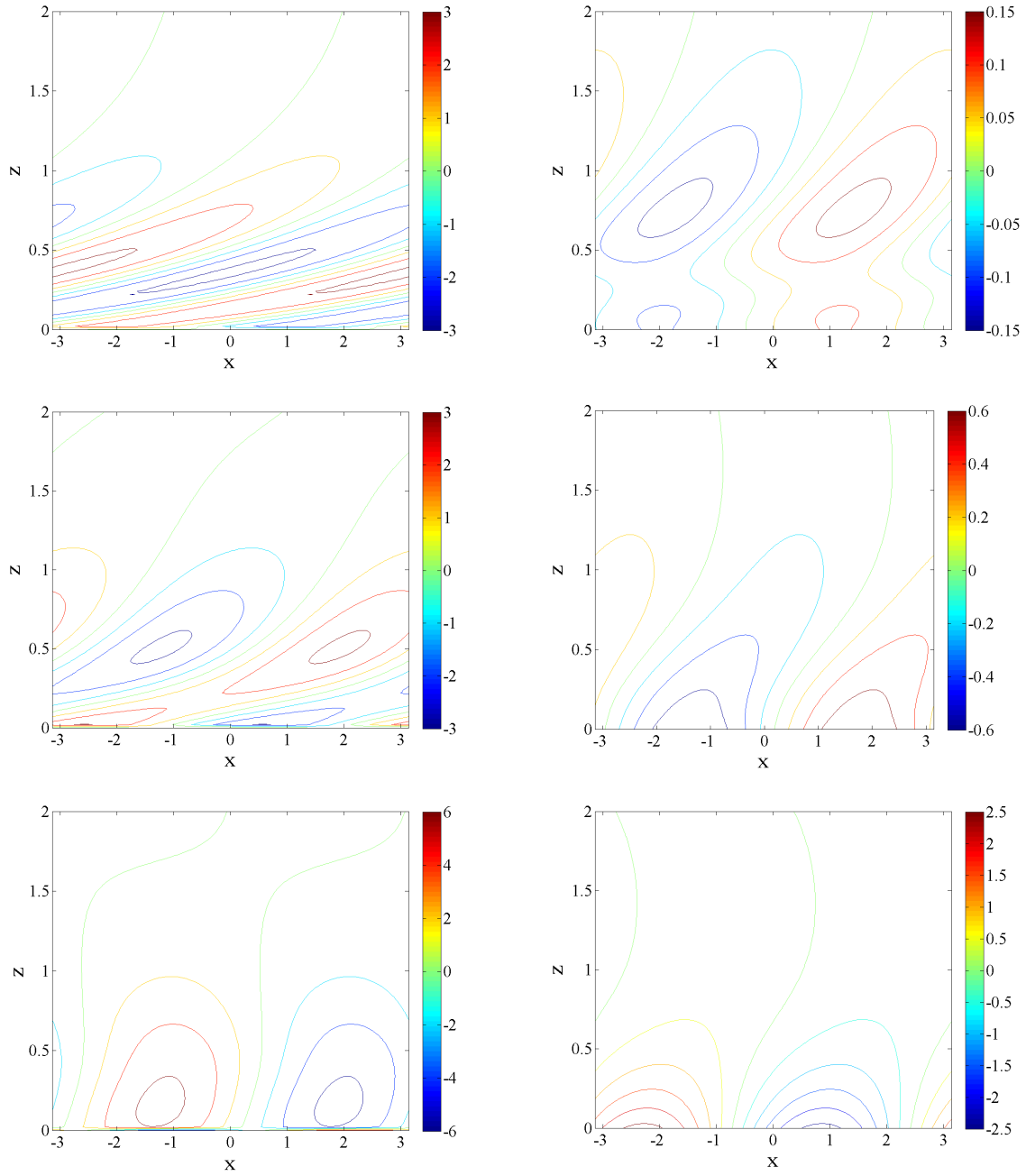
Figure 22: As for Figure 21 but for near neutral wavelength $r = 0.45$
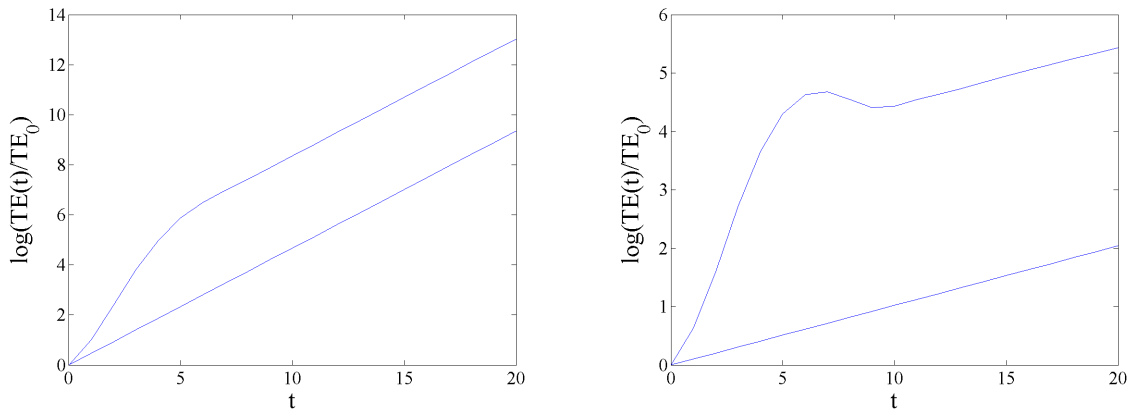
Figure 23: Log total energy growth against time using the leading singular vector as the initial perturbation for $r = 0.22$ (left) and $r = 0.45$ (right). Log GNM energy growth also shown in each plot by the straight lines. All variables non-dimensional.